



Management and Components for Advanced Lead-Acid Batteries

Angel Kirchev

► To cite this version:

Angel Kirchev. Management and Components for Advanced Lead-Acid Batteries. Theoretical and/or physical chemistry. Université de Grenoble, 2013. tel-03579565

HAL Id: tel-03579565

<https://cea.hal.science/tel-03579565>

Submitted on 18 Feb 2022

HAL is a multi-disciplinary open access archive for the deposit and dissemination of scientific research documents, whether they are published or not. The documents may come from teaching and research institutions in France or abroad, or from public or private research centers.

L'archive ouverte pluridisciplinaire **HAL**, est destinée au dépôt et à la diffusion de documents scientifiques de niveau recherche, publiés ou non, émanant des établissements d'enseignement et de recherche français ou étrangers, des laboratoires publics ou privés.



UNIVERSITÉ DE GRENOBLE

MEMOIRE

en vue de l'obtention d'une

HABILITATION à Diriger les Recherches DE L'UNIVERSITÉ DE GRENOBLE

Spécialité : Matériaux et Génies des Procèdes

Arrêté ministériel : 7 août 2006

Présentée par

« Angel KIRCHEV »

préparée au sein du Laboratoire CEA/DRT/LITEN/DTS/LSE,
dans l'École Doctorale : IMEP2

Gestion et Composants pour Accumulateurs au Plomb Avancés

Habilitation soutenue publiquement le « **02.07.2013** »,
devant le jury composé de :

M, Patrice, SIMON

Professeur des Universités Paul Sabatier, Toulouse, Président

M, François, HUET

Professeur des Universités Pierre et Marie Curie, Paris, Rapporteur

M, Emmanuel, ROCCA

Maitre de Conférences-HDR, Université de Lorraine, Nancy, Rapporteur

Mme, Christine, LEFROU

Maitre de Conférences-HDR, Grenoble INP, Rapporteur

M, Patrick, MOSELEY

Docteur, Président de l'ALABC, ILZRO, Durham USA, examinateur

M, Detchko, PAVLOV

Professeur et Membre de l'Academie Bulgare des Science, Sofia
Bulgarie, examinateur



Abstract

The manuscript presents a series of works aimed to optimise the performance of the valve-regulated lead-acid battery (VRLAB) in terms of lifetime and energy and power density. The first direction includes the development of various battery management solutions based on the detailed comprehension of the lead-acid battery electrochemistry. The oxygen recombination current and the oxygen cycle efficiency were measured using a custom-made gassing rate monitoring system. The correlation between the proposed model and the measured data showed that the oxygen cycle is gas-diffusion limited process. It is demonstrated that the integration of reference electrodes for positive plate potential regulation during the charge is one of the best strategies for control over the oxygen cycle and prevention of the thermal runaway phenomenon. Further, the mechanism of the pulse charge of the lead-acid battery was studied separately on the positive and on the negative plate using electrochemical impedance spectroscopy. It is concluded that the pulse charge with a frequency close or equal to the characteristic frequency of the charge reaction leads to an electrochemical resonance corresponding to a maximum of the charge acceptance. The impact of the electrolyte on the positive plate electrochemistry is studied on small-scale “Planté” electrodes and on traction positive plates. It is found that sulphuric acid electrolytes with concentration higher than 5mol/l cause a passivation of the lead dioxide electrode. QCM electrode studies revealed that the passivation is caused by a solid-state PbO_2 reduction mechanism taking place with proton insertion. The improvement of the specific power and energy of the battery was accomplished by the replacement of the traditional grids with innovative carbon honeycomb current collectors. They offer high ratio between the surface area of the grid and the quantity of the active materials as well as excellent compatibility with the AGM technology.

Résumé

Ce mémoire présente un recueil de travaux ciblant l'amélioration des performances des accumulateurs au plomb étanches de type AGM-VRLAB en termes de la durée de vie et de densités de puissance et d'énergie. La première direction comprend le développement de solutions de gestion (BMS) basées sur l'électrochimie détaillée de la batterie. Le courant lié à la recombinaison de l'oxygène et l'efficacité du cycle de l'oxygène ont été mesurés à l'aide d'un système de mesure du dégazage pendant le cyclage et la surcharge de l'accumulateur. La corrélation entre le modèle proposé et les données expérimentales a montré que la réaction de recombinaison est limitée par la diffusion de l'oxygène. J'ai montré que l'utilisation des électrodes de référence intégrées aux cellules d'accumulateurs est une très bonne stratégie de contrôle du cycle de l'oxygène qui permet d'avoir une prévention continue contre les risques d'emballlement thermique en fin de charge. J'ai pu montrer qu'une charge galvanique pulsée effectuée à une fréquence proche de la fréquence caractéristique de la réaction de transfert de charge de l'électrode positive ou négative permettait d'obtenir une acceptation de charge optimale par un effet de « résonance électrochimique ». L'impact de l'électrolyte sur l'électrochimie du système $\text{PbO}_2/\text{PbSO}_4/\text{H}_2\text{SO}_4$ a été étudié sur des électrodes de type « Planté » ainsi que sur des plaques positives d'accumulateurs de type « traction ». J'ai prouvé que pour électrolytes de concentration supérieure à 5mol/L le dioxyde de plomb devient passif. Des études effectuées par méthode couplée EQCM ont révélé que la passivation est liée à la réaction de réduction de PbO_2 en phase solide provenant d'une insertion des protons dans le volume des particules de PbO_2 . Finalement, l'amélioration de la puissance et de l'énergie de l'accumulateur au plomb a été obtenue via le remplacement des grilles traditionnelles par des collecteurs de courant de carbone en nid d'abeille possédant une grande surface géométrique.

Contents

Chapter 1	
Introduction – the lead-acid battery across three centuries	3
Chapter 2	
Management of Advanced Lead Acid Batteries	5
2.1. Oxygen Recombination in AGM-VRLA cells	6
2.2. Thermal Runaway during the charge of AGM-VRLA batteries	13
2.3. Integration of Reference Electrodes in VRLA cells for Advanced Battery Management.....	14
2.4. Pulse charge – an interaction between Faradic and capacitive battery properties	17
2.4.1. Impedance of the positive plate	19
2.4.2. Impedance of the negative plate	21
2.4.3. Electrochemical resonance	24
Chapter 3	
Components for Advanced Valve-Regulated Lead Acid Batteries	26
3.1. The electrolyte as the third active material	26
3.1.1. The Pb/PbO ₂ /PbSO ₄ /H ₂ SO ₄ electrode system	27
3.1.2. Influence of the sulphuric acid concentration on the positive plate performance	30
3.1.3. Mechanism of the solid state passivation of the lead dioxide electrode	33
3.2. Carbon honeycomb grids for advanced positive and negative plates	37
Chapter 4	
Conclusions	39
Chapter 5	
Research Perspectives	40
References	43
Curriculum Vitae	46
List of publications in periodic journals	49
List of publications in conference proceedings	50
Patent applications	51
Conference presentations	51
Poster communications	53
Acknowledgements	54

Management and Components for Advanced Lead-Acid Batteries

Gestion et Composants pour Accumulateurs au Plomb Avancés

Chapter 1

Introduction – the lead-acid battery across three centuries

The lead acid battery was invented by the French scientist Gaston Planté in 1859 and demonstrated at the French Academy of Sciences a year latter in 1860. During the following three decades this energy storage system was rapidly improved for the time being, becoming the power source of the first electric vehicles and the support of the first DC electric grids.

Now, century and a half latter, the lead-acid battery still holds an impressive energy storage market share despite the enormous research and development efforts to deliver better storage systems. In terms of energy storage capacity units, this share is almost 90% for 2011 [1].

Several key advantages stand behind the successful story of the lead-acid battery:

- **Manufacturing capability**: the lead-acid cells and mono-blocks (two to six cells in series sharing a common casing) are manufactured at high production rates. For example, a small independent French SLI (start-lightning-ignition) lead-acid battery manufacturer will a staff of less than 200 persons (ranking it as a PME type of company) is able to produce annually about 3 million of units with an average storage capacity of 0.5-1kWh. Such a production level is equivalent to about 100 000 – 200 000 packs for electric or plug-in hybrid vehicles annually. The electrochemical capacity of a unit lead-acid cell varies from 2-3 to 10000-11000Ah making even the installing of large-scale energy storage systems relatively simple task.
- **Raw materials**: the key component of the lead-acid battery is the lead metal. Due to its health and environmental hazard nature, the lead is used almost exclusively (with small exceptions) for lead-acid battery manufacturing. The absence of industry able to offer competitive market prices for substantial quantities of this metal keeps its cost relatively low and constant over long periods.
- **Recycling**: the lead-acid battery is comprised of very limited number of components - lead metal with minor alloying additives, lead sulphate and lead oxides, plastics (polypropylene and ABS from the boxes, polyethylene or PVC from separators), glass fibre and sulphuric acid. These components are easy separated and completely recycled (especially the lead) back into batteries with considerable profit making this industry en example for durable and self-sustainable system.
- **Safety of operation**: the lead-acid battery is very robust system. It is able to operate in very large temperature scale – from -30°C up to 60-80°C (depending on the properties of the plastics casing), tolerating abusive phenomena like external short-circuiting or mechanic shocks. Long strings of cells in series can operate without any particularities due to the intrinsic ability of the battery for cell balancing due to the high tolerance for overcharging.

All these factors make the lead-acid battery the most affordable energy storage system on the market. Despite its strong sides, the lead acid battery has some important drawbacks making this system more and more unattractive for numerous applications:

- Low energy density: the lead is an element from the bottom of the periodic table with relatively poor electrochemical equivalent. Together with its limited “electrochemical” utilization in the battery, this results in energy density of the final product in the range of 35Wh/kg (+/-5Wh/kg depending on the size and the design of the cells).
- Limited power density: the high specific gravity of the lead and its compounds are also the main reason for the limited power density of the system.
- Short cycle life: the charge discharge cycling at different regimes (respectively the use of the lead-acid battery in different application) is associated with evolution of different degradation phenomena in the positive and the negative plates. Amongst them, the most severe phenomena are the positive active material softening and shedding and the corrosion of the positive grids. Usually the attempt to increase the cycle life changing the electrodes and cell design results in decease of the specific energy and the specific power of the battery or appearance of new problems and technological challenges.

Dr Kirchev spent the last dozen of years in attempt to understand better the mechanisms of manufacturing, operation and degradation of different types of lead-acid batteries. Stepping on the obtained experience, the development of different solutions for overcoming of the above-mentioned problems has been started in the Laboratory for Storage of Electricity of CEA-LITEN. These solutions can be divided in two groups:

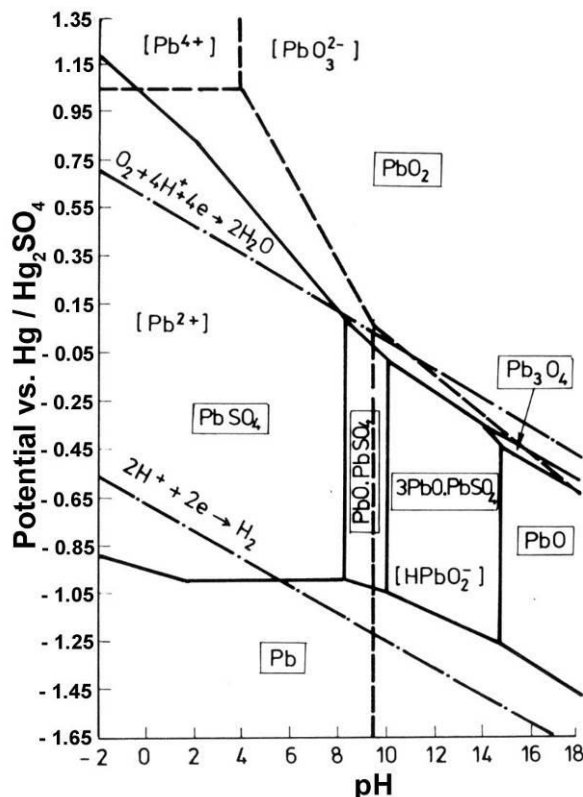
- Battery management solutions: the lead-acid battery is an extremely versatile storage system able to serve in numerous different applications. However each application has its specifics impacting in a different way the lead-acid battery electrochemistry. The aim of the battery management is to find the best match between the application specifics and the electrochemical phenomena. In this way the battery lifetime can be improved markedly.
- Battery component solutions: in order to improve the performance of the lead-acid battery it is important to replace some of its components. For example the lead-alloy grids can be replaced with more advanced structures allowing higher active mass utilization and longer cycle life. In other case, new components should be added to the lead-acid cells in order to apply more precise battery diagnostics or charge algorithms.

Chapter 2

Management of Advanced Lead Acid Batteries

A key drawback of the classical lead-acid battery, often denoted as “flooded” or “vented” type, is the necessity of maintenance in the form of periodic refill with water which is lost due to the processes of hydrogen and oxygen evolution during the charge and the self-discharge. The origin of these phenomena is in the lead-acid battery thermodynamics – the equilibrium electrode potentials of the reactions of energy storage ($\text{Pb}/\text{PbSO}_4/\text{H}_2\text{SO}_4$ and $\text{PbO}_2/\text{PbSO}_4/\text{H}_2\text{SO}_4$ electrodes) are far beyond the equilibrium potentials of the hydrogen and the oxygen electrodes as it is illustrated in the Pourbaix diagram of the system lead – sulphuric acid (Figure 2.1) [2].

Fig. 2.1. Potential / pH diagram of the system lead – sulphuric acid [2].



The problem with the water loss can be solved in several different ways. In one approach the design of the flooded lead-acid cells can be kept the same, just adding catalytic vent-plugs or automatic water top-up systems [3]. The alternative approach resulted in the development of the so-called Valve-Regulated Lead-Acid Batteries (VRLA battery), also denoted as Sealed Lead-Acid Batteries (SLA battery). In the VRLA battery the electrolyte is immobilized either in the form of a gel using suitable jellifying agents (fumed silica, silica gel etc...) or absorbed in a thick glass-fiber mat separator (AGM – absorptive glass mat) and each cell is kept sealed using a pressure release valve. This change in the battery design results in the appearance of internal oxygen cycle preventing the water loss. In order to have a maintenance-free operation over sufficient periods of time (preferentially the whole battery lifetime) the use of suitable charge management became mandatory, because improper charging would result in poor oxygen cycle efficiency and corresponding rapid battery dry out. From the other hand too intensive oxygen cycle operation hinders the complete recharge of the negative plates and thus

the negative active material becomes more susceptible to sulfation [4]. The immobilisation of the electrolyte and the sealing of the cells eliminates the physical access to the electrolyte making impossible to use the traditional lead-acid battery diagnostics using specific gravity measurements. This new variety of problems associated with the advanced lead-acid batteries operation led to a necessity to search for innovative battery management solutions.

2.1. Oxygen Recombination in AGM-VRLA cells

The comprehension of the electrochemical kinetics of the reactions taking place in the battery is the background behind each Battery Management System (BMS). This statement is particularly relevant in the case of the oxygen recombination process in the AGM-VRLA batteries. The oxygen recombination process together with the charge management of VRLA batteries were the main subjects of the PhD thesis of Dr. Angel Kirchev.

The AGM separator is a paper-like material made of wet-laying of glass microfibers (typically a borosilicate type) with a very small contact angle of wetting by sulphuric acid electrolytes. The resulting separator structure shown in Figure 2.2 [5] absorbs and retains almost completely the lead-acid battery electrolyte due to the action of the capillary forces. The AGM separator has larger pores in direction perpendicular to the plane of the separator sheet (z-direction) and smaller pores along the plane of the sheet (x and y directions) due to the nature of the fibre laying process. When the volume of the AGM separator is partly filled with electrolyte, the largest pores (those in the z-direction) are preferentially void due to the lowest capillary pressure there. These empty pores are able to transport easy gaseous oxygen evolved at the positive plate across the separator to the surface of the negative plate. On the negative plate the oxygen recombines with protons forming water and heat. The whole process is often denoted as oxygen cycle, closed oxygen cycle or internal oxygen cycle. During the operation of the oxygen cycle, the negative plate of the battery is working as a gas-diffusion electrode. Here the oxygen diffusion through the electrolyte layer wetting the surface of the lead crystals limits the electrode kinetics. Figure 2.3 presents a scanning electron micrograph of the negative active material and a scheme of pore partly filled with electrolyte. Following the route of the lowest possible capillary pressure it is accepted that the gas-filled pore is quasi-cylindrical. On the other hand the pore walls can be considered as thin liquid films separating the gas phase and the lead metal. The thickness of these electrolyte films will be defined by the balance between the capillary pressure inside the pore and the “disjoining pressure” in the thin liquid layer. The latter corresponds to the force of interaction (repulsion or attraction) between both surfaces of the thin liquid layer. Combining the data from the mercury intrusion porosimetry and the thermodynamics of the thin liquid films (especially the DLVO theory) it was possible to evaluate the thickness of the electrolyte gas diffusion layer as well as its surface as a function of the electrolyte saturation of the active block. The calculated data presented in Figure 2.5 show that the thickness of the gas diffusion layer should be between 5 and 15nm in the typical electrolyte saturation levels (85-95%) and relatively small fraction of the NAM surface is involved in the oxygen recombination process.

The process of the oxygen recombination in VRLA cells was studied experimentally combining galvanostatic polarisation and cyclic voltammetry with simultaneous monitoring of the gas flow escaping the cell during its overcharge. The experimental setup is presented in Figure 2.6. The cell is immersed in thermostated water bath and the gas flow is detected as number of bubbles per unit of time by the gassing rate monitoring system developed in the Lead-Acid Battery Department of IESS-BAS.

Fig. 2.2. Scanning electron micrographs of AGM separator Hollingsworth & Vose 440g/m² [5].

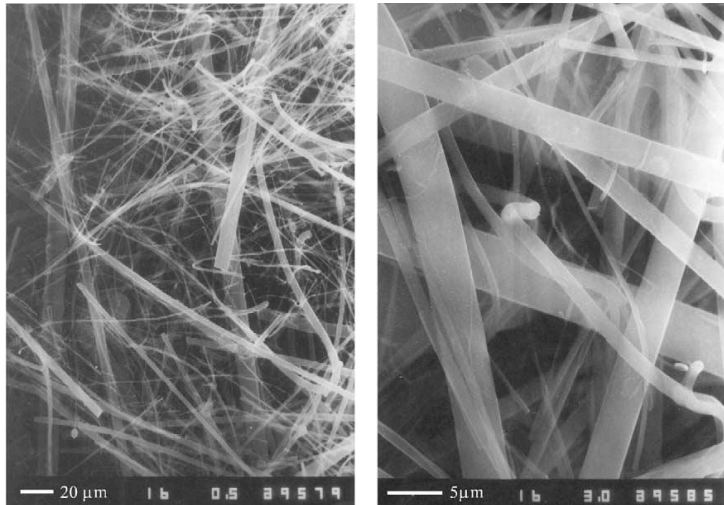


Fig. 2.3. SEM of negative active material morphology and model of the cross-section of NAM pore partially filled with electrolyte [6].

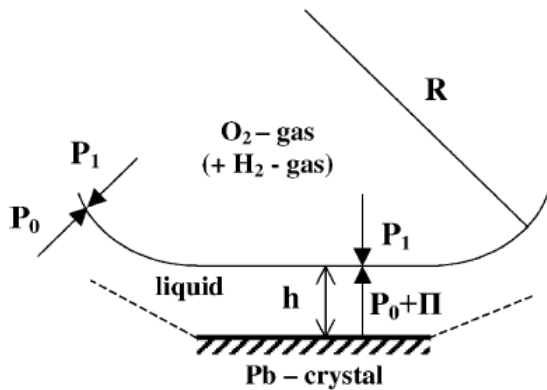
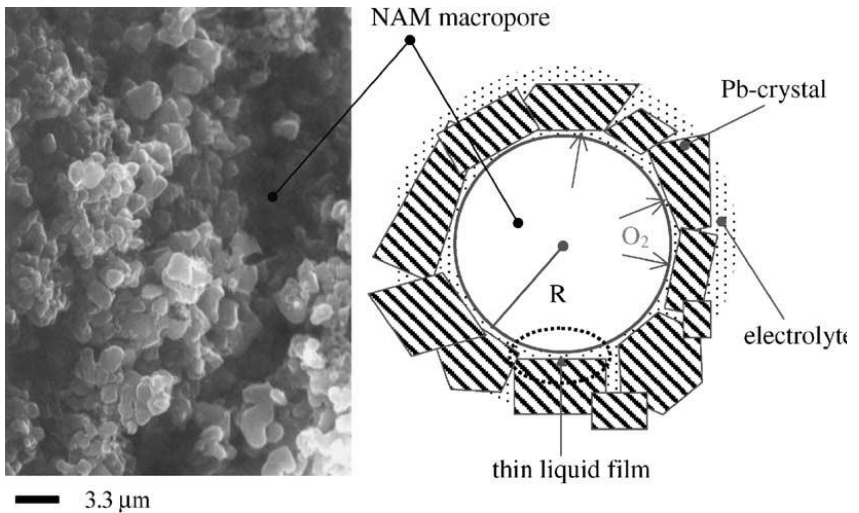
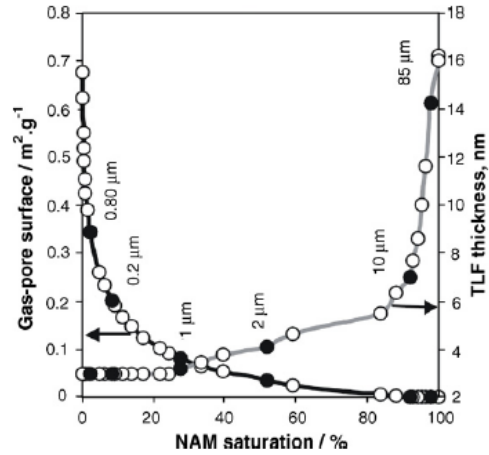


Fig. 2.4. Schematic representation of the balance of forces determining the stability of the wetting film formed in an open gas pore in NAM [6].

Fig. 2.5. Dependence of the area of the gas-filled NAM pores (black curve) and wetting film thickness (gray curve) on the electrolyte saturation of NAM [6].



The non-stationary kinetics of the oxygen recombination process was studied at galvanostatic conditions overcharging 1.6Ah AGM-VRLA cells applying staircase-like current profile [6]. Considering the oxygen diffusion through the thin liquid film wetting the surface of the lead

crystals, the oxygen recombination current was calculated as function from the moment of the increase of the overcharge current using the initial and boundary conditions illustrated in Figure 2.7:

$$I_{rec} = -4FSD \left(\frac{\partial c}{\partial x} \right)_{x=0} = 4FSD \left(\frac{c_3 - c_4}{h} - \frac{c_4 - c_2}{\sqrt{\pi D t}} \right) \quad (2.1)$$

Where F is the Faraday's constant, S is the surface area of the wetting film and D is the oxygen diffusion coefficient in the electrolyte. In the case of overcharge the total current can be presented as a sum of the oxygen recombination current and gassing current corresponding to hydrogen and oxygen leaving the cell $I = I_{rec} + I_{gas}$. The latter corresponds to the gas flow measured by the equipment illustrated in Figure 2.6. Since the output of the used gassing rate monitoring system has a discrete character (it measures number of bubbles per unit of time) it is much more convenient to use the integral form of equation 2.1 and to analyze the cumulative gas volume as a function of time or the cumulative number of bubbles detected by the system which is a parabolic function of the square root of time $N(t^{1/2})$:

$$N(t) = a_2 t + a_1 t^{1/2} \text{ or } N(z) = a_2 z^2 + a_1 z \quad (2.2)$$

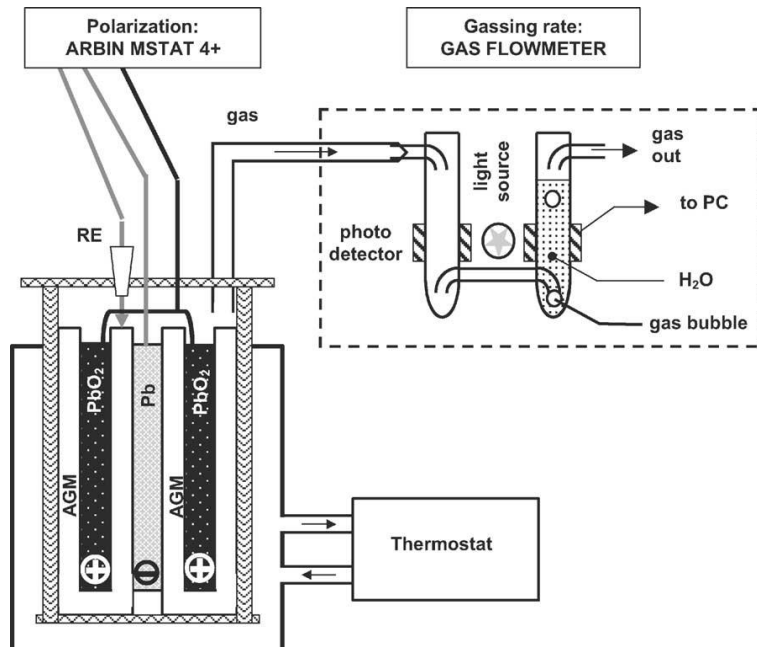


Fig. 2.6. Scheme of the experimental setup used in the oxygen recombination studies [6].

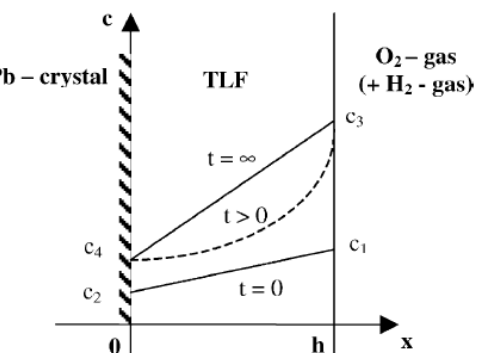
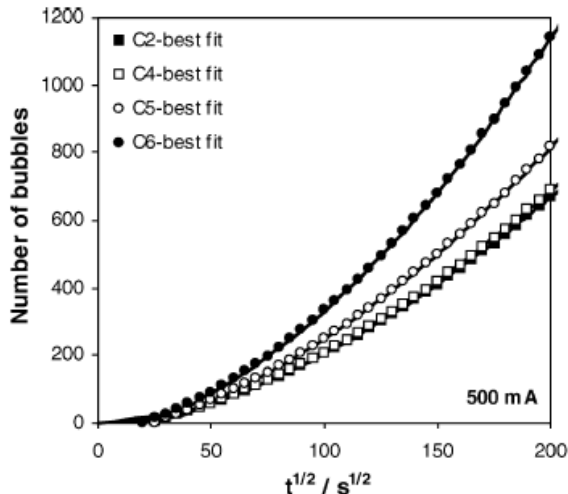


Fig. 2.7. Initial and boundary conditions for Fick's equation. The symbol "c" denotes the oxygen concentration in the electrolyte film, "x" and "t" are the distance from the lead surface and the time [6].

Figure 2.8 presents the correlation between the experimental data and Equation 2.2 in terms of cumulative number of bubbles vs. the square root of time. In this particular experiment the overcharge current is increased from 450 to 500mA (nominal capacity of the cells 1.6Ah). It can be seen a good match between the data and the suggested gas-diffusion kinetics.

Fig. 2.8. Dependence of the cumulative number of bubbles on the square root of time and the best fits obtained using Equation 2.2 [6].



The complete charge of VRLA battery takes typically several hours. In the end of this period the current density is usually kept low either choosing low end of charge voltage or a small constant current. Under these conditions one can consider the kinetics of the oxygen cycle as stationary, i.e. small variations of the current are accompanied by small variations of the electrode potentials, as well as by slow increase of the state of charge being close to 100%.

The stationary kinetics of the oxygen cycle in cell from the above-mentioned type was studied using linear cycling voltammetry with a sweep rate of $20\mu\text{V/s}$ in the negative plate potential range -1.05 to -1.30V vs. $\text{Hg}/\text{Hg}_2\text{SO}_4/\text{H}_2\text{SO}_4$ reference electrode (MSE) [7]. The experiments were carried in overcharge mode using the gassing rate monitoring system at two different electrolyte saturation levels – 83% ($20\mu\text{V/s}$) and 100% ($60\mu\text{V/s}$). The latter conditions were achieved adding an excess of water in the cell thus blocking the oxygen transport across the AGM separator and allow evaluating the dependence of the hydrogen evolution current on the negative plate potential. Figure 2.9 illustrates the voltammetry data of the cell with 83% and 100% saturation at 15°C . The calculated current of electrochemical oxygen recombination correlates well with an equation of mixed charge transfer and diffusion kinetics [8]:

$$\varphi^- = \frac{RT}{\alpha nF} \ln \frac{I_0}{I_d} + \frac{RT}{\alpha nF} \ln \left(\frac{I_0}{I_d} - 1 \right) \quad (2.3)$$

where α is the charge transfer coefficient, I_0 is the exchange current and I_d is the limiting diffusion current.

Combining the gassing rate data and the voltammetry results at both saturation levels it was possible to distinguish the gassing current, the total current of oxygen recombination and the partial current of electrochemical oxygen recombination as well as to evaluate the total and the “electrochemical” oxygen recombination efficiency. Figure 2.10 presents the obtained data for the case of 15°C . It can be seen that up to -1.2V vs. MSE there is any gassing. Beyond this value the efficiency of the oxygen cycle starts to decrease. The observed small difference between the electrochemical and the overall oxygen cycle efficiency indicates that the process takes place preferentially by the so-called “electrochemical” mechanism:



The increase of the temperature brings substantial changes in the mechanism of the oxygen recombination process. The voltammetry curves presented in Figure 2.11 show a remarkable difference between the gassing current measured at 83% saturation and the hydrogen evolution current measured at 100% saturation.

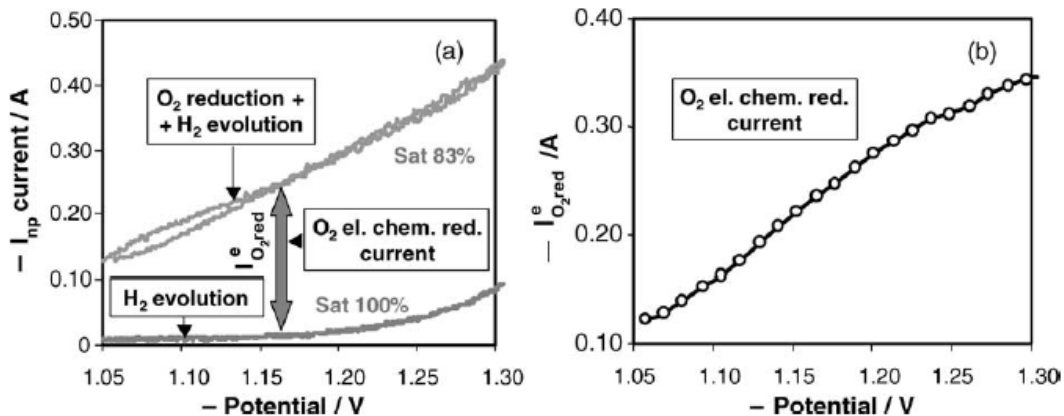


Fig. 2.9. Cyclic voltammetry plot of a completely charged VRLA cell (1.5Ah) with saturation 83% and 100% at 15°C (a) and calculated volt-ampere plot of the electrochemical oxygen recombination process [7].

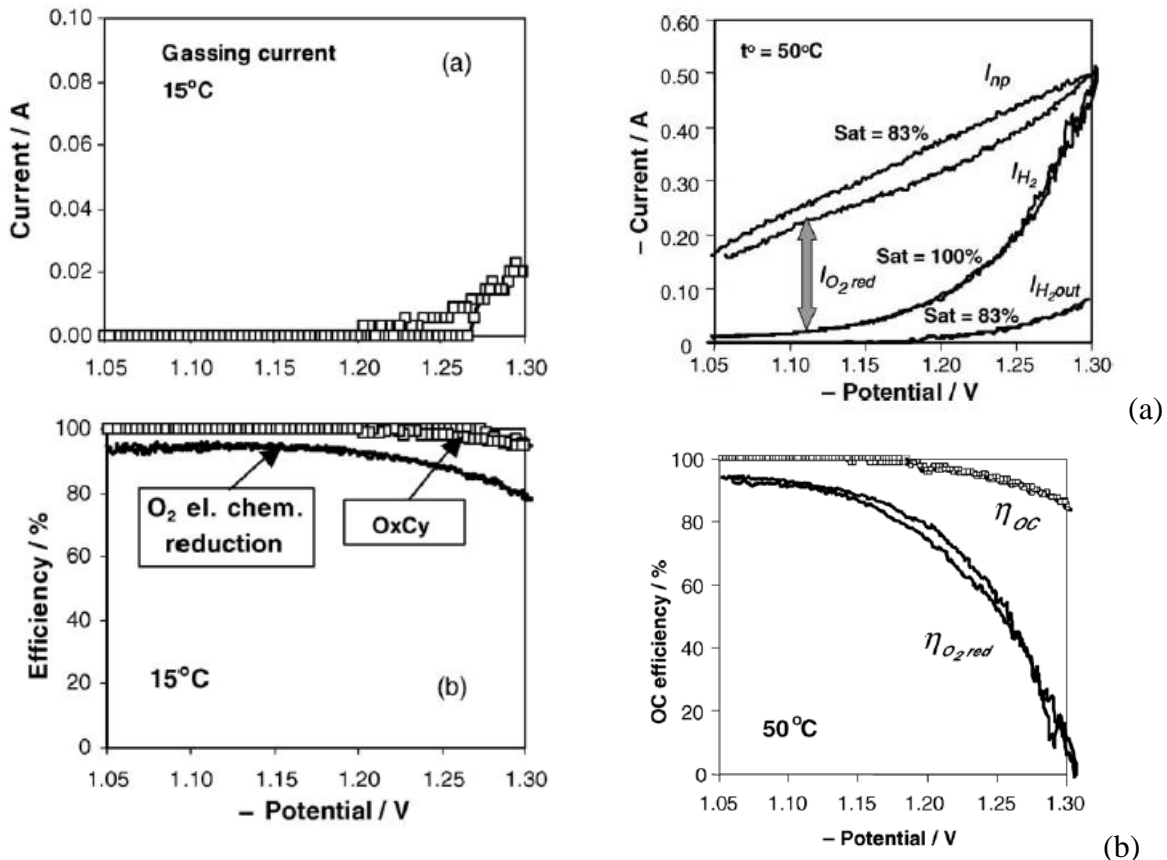


Fig. 2.10. Gassing rate current and oxygen cycle efficiency as a function of the negative plate potential at electrolyte saturation 83% and 100% at 15°C [7].

Fig. 2.11. Cyclic voltammetry plots (a) and oxygen recombination efficiency (b) of cell operating at 50°C [7].

The latter results in a great difference between both types of oxygen recombination efficiency (Figure 2.11b), which supposes that the process of oxygen recombination is linked with the hydrogen evolution reaction. A scheme explaining such a connection based on the voltammetric and gas flow measurements is shown in Figure 2.12.

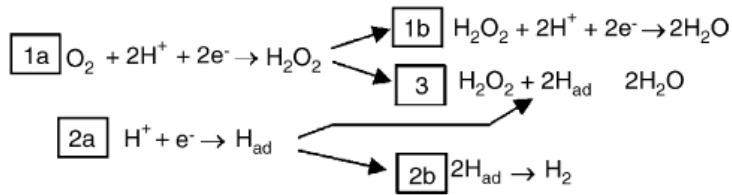
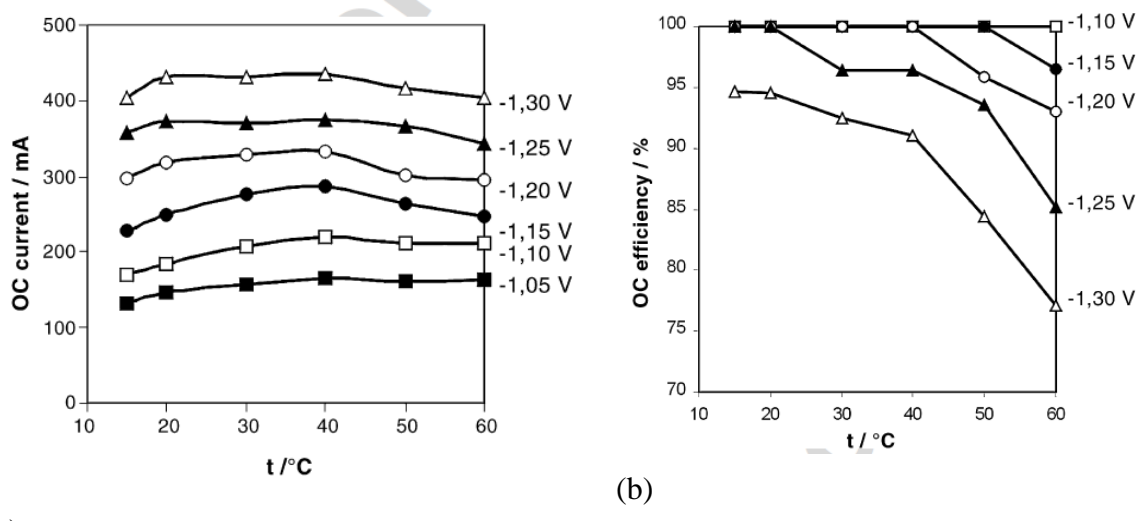


Fig. 2.12. Scheme of the oxygen cycle reactions involved in the reduction of the oxygen and the evolution of hydrogen at negative plate of VRLA cell [7].

During the ageing, each VRLA battery experience water loss due to two irreversible processes regardless of the charge management. These are the positive grid corrosion and the hydrogen evolution. Thus with the time, the saturation of the AGM separator decreases leading to changes in both the oxygen cycle current and the oxygen cycle efficiency. VRLA batteries are often used in various outdoor applications or in close compartment next to internal combustion engines or power electronics. In such cases its operating temperature increases which may alter the electrochemical kinetics of the oxygen recombination.

Figure 2.13 presents the influence of the temperature on the oxygen recombination current and on the oxygen cycle efficiency for various values of the negative plate potential in the case of 83% saturation of the active block [9]. Surprisingly, the temperature does not influence markedly the current of the oxygen recombination process at a fixed value of the electrode potential. According to the proposed gas-diffusion approach, the recombination process depends on thickness of the wetting electrolyte film, the oxygen diffusion coefficient in the electrolyte and the oxygen solubility. From one hand, the increase of the temperature will increase the value of the diffusion coefficient. From the other, the oxygen solubility decreases and so does also the thickness of the wetting electrolyte film. The latter is due to the decrease of the surface tension at higher temperatures. Contrary to the oxygen recombination rate, the efficiency of the oxygen cycle depends strongly on the temperature in an exponent-like fashion. The latter is due to the kinetics of the concurrent process of hydrogen evolution which follows closely both Tafel and Arrhenius behaviour.



(a)

Fig. 2.13. Temperature dependence of the oxygen cycle current (a) and the oxygen cycle efficiency (b) at 83% electrolyte saturation of the active block (1.5Ah cell) [9].

These results indicate that the VRLA operation at temperature 35-40°C should be accompanied with half-cell potential monitoring in order to minimize the drying out of the battery and yet to achieve a complete recharge of the negative plate in order to avoid a sulfation of the active material. A potential close to -1.20V vs. MSA is a good trade-off between the oxygen cycle efficiency and negative plate recharge capability because it ensures enough polarisation vs. the open circuit potential of the Pb/PbSO₄ electrode (~ -1V vs. MSE).

The impact of the electrolyte saturation of the active block on the rate and the efficiency of the oxygen cycle is presented in Figure 2.14 for the case of negative plate potential equal to -1.20V vs. MSE. It can be seen that below 93% saturation of the active block, the oxygen recombination current starts increasing rapidly and the oxygen cycle efficiency trends to 100%. In order to explain this particular value of the electrolyte saturation, the pore-size distributions of the AGM separator and the negative active material were compared using mercury intrusion porosimetry. When the electrolyte saturation decreases due to the water loss, the evacuation of the liquid starts from the largest pores where the capillary pressure is lowest. Taking into account this assumption, the pore radius corresponding to 93% electrolyte saturation was calculated and denoted in the pore size and pore surface distribution curves presented in Figure 2.15.

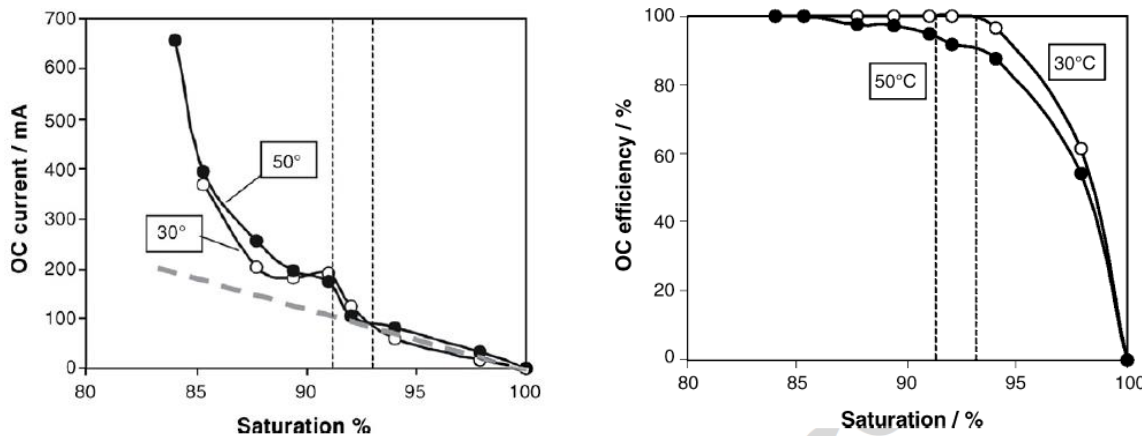


Fig. 2.14. Influence of the electrolyte saturation on the oxygen recombination current and the oxygen cycle efficiency at $\varphi^- = -1.20V$ vs. MSE (1.5Ah cell) [9].

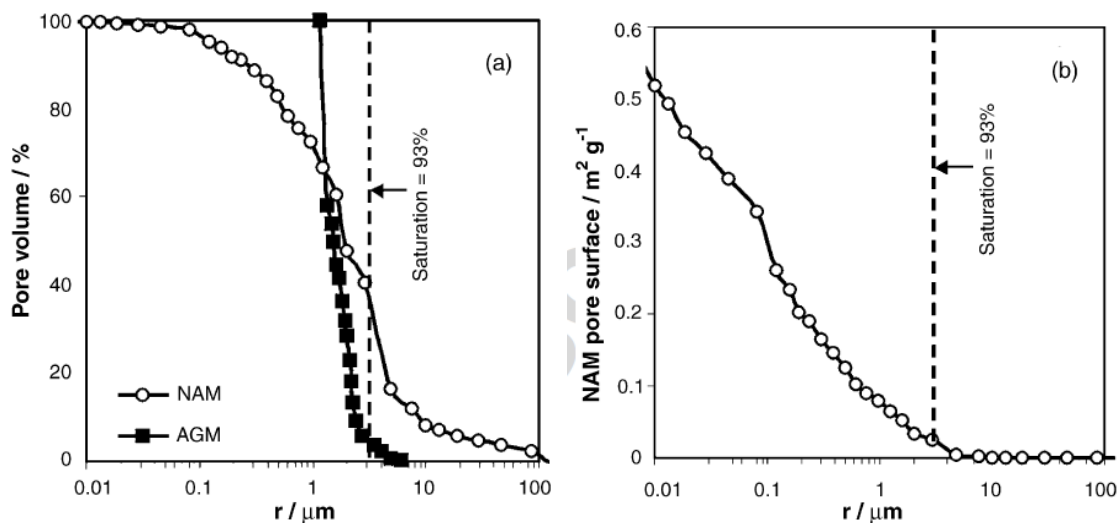


Fig. 2.15. Cumulative pore volume as a function of the pore radius for NAM and AGM and (b) pore surface as a function of the pore radius for NAM. The dotted line notes 93% electrolyte saturation of the active block [9].

The results from this analysis show that a decrease of the saturation beyond 93% starts involving parts of the negative active material with considerably larger specific surface area explaining well the rapid increase of the oxygen cycle current. Moreover, the higher capillary pressure in the smaller pores leads to thinner electrolyte wetting films and faster oxygen diffusion through them, making the smaller pores more “reactive” for the process of the oxygen recombination.

2.2. Thermal Runaway during the charge of AGM-VRLA batteries

The main safety issue related to the operation of the VRLA batteries is the so-called “thermal runaway”. The phenomenon is a direct consequence of the oxygen cycle operation since the latter converts the electricity injected in the battery in heat via different mechanisms (Joule heat, reactions heat etc...). The latter means that it **can be observed only** in the end of the battery charge and during its overcharge. The impeded heat exchange is the main accelerator of the thermal runaway, making larger energy storage installations particularly susceptible to it. The kinetics of the thermal runaway was studied using a setup similar to the one depicted in Figure 2.6 using cells with two positive and three negative plates (nominal capacity of 4Ah), which were placed in adiabatic containers and connected with the same gassing rate monitoring system. Thermocouples were installed inside the cells measuring the internal temperature in close proximity to the negative plate where the main part of the heat is generated [10].

Figure 2.16 presents the oxygen cycle kinetics observed at cell continuously overcharged with 2.40V. This is a typical value for constant voltage charge mode for most of the VRLAB technologies. The evolution of the thermal runaway can be divided in four stages. In the beginning of the overcharge, the negative plate responds more rapidly to the polarisation however, the oxygen coming from the positive plate changes the negative plate potential almost to its open circuit value. This continues until the maximum value of the positive plate potential is reached. In the same time both the current and the temperature increase gradually up to 2A (C/2h) and 40°C in the middle of the stage B. Beyond this point the current starts increasing rapidly followed by the temperature. The increasing overcharge current results in oxygen evolution rate exceeding the limiting current of the oxygen recombination, while the high temperature decreases the hydrogen overvoltage. As a result the cell starts venting gas. The release of gaseous oxygen and hydrogen from cell already corresponds to another form of energy conversion and the heat generation inside the cell starts decreasing. This is followed by a decrease of the current and the temperature during the stages C and D. A calculation of the simplified thermal balance of the cell during this thermal runaway is presented in Figure 2.17. It can be seen that the process is triggered almost exclusively by the chemical reaction heat, i.e. by the reactions involved in the oxygen recombination process. The Joule heat starts contributing markedly in the latter stages of the thermal runaway. A clear evidence for the importance of the chemical reactions involved in the thermal runaway was found during the post-mortem analysis of the positive and negative plates. Since the cells operate in overcharge mode any or very small quantity of PbSO₄ should be found. This suggestion was confirmed only at positive plate where the volume part of the β-PbO₂ was as high as 97-98%. The phase composition of the negative plates after the thermal runaway included substantial quantities of PbSO₄ and 3PbO.PbSO₄.H₂O, which can be a result from the oxidation of the lead by the oxygen or by the intermediates involved in the oxygen recombination. The build-up of such phases increases the cell resistance and as a consequence, the thermal runaway can not be repeated with the same magnitude at the same values of the cell voltage.

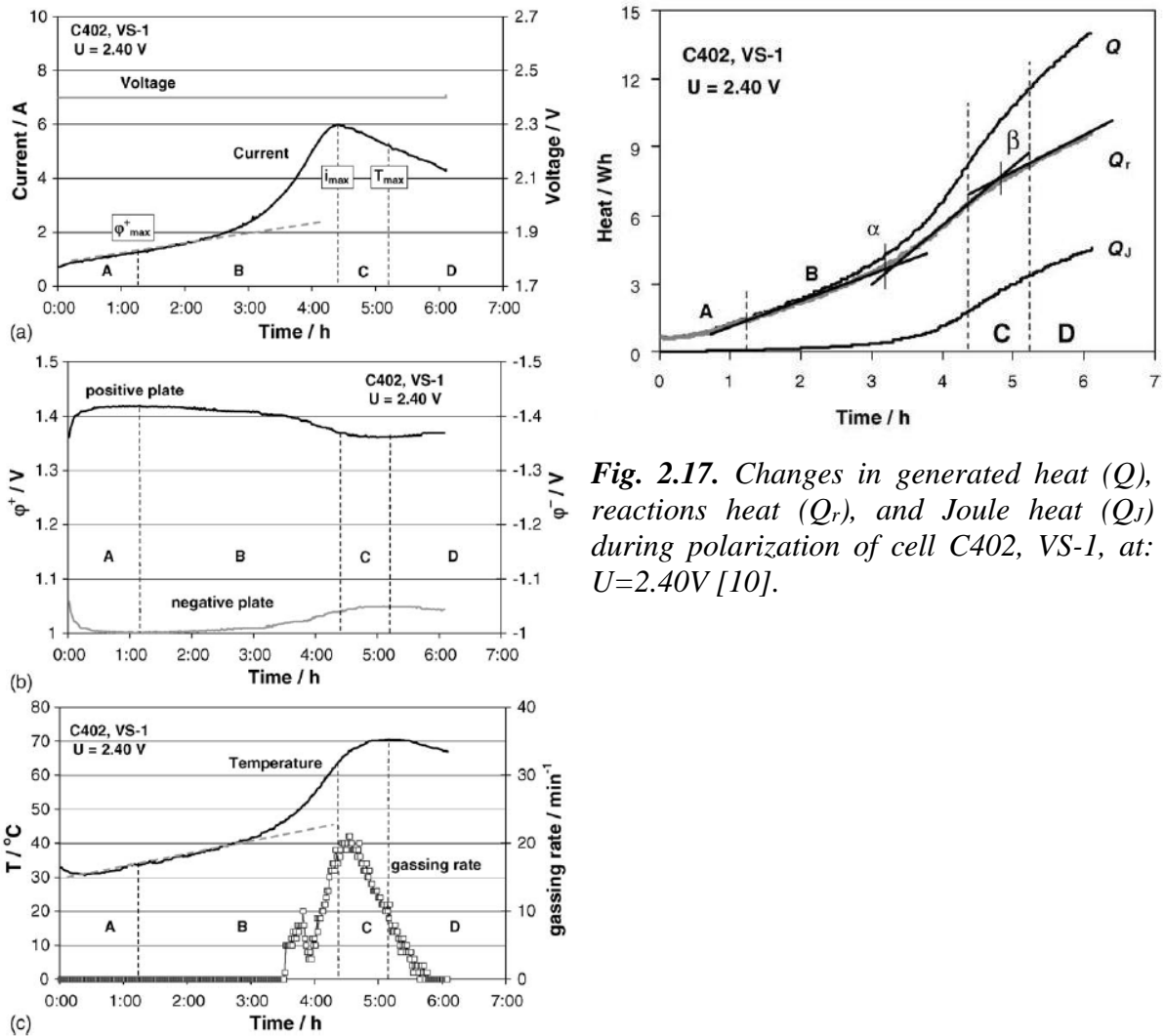


Fig. 2.17. Changes in generated heat (Q), reactions heat (Q_r), and Joule heat (Q_J) during polarization of cell C402, VS-1, at: $U=2.40V$ [10].

2.16. Cell current, positive and negative plate potentials (vs. $\text{Ag}/\text{Ag}_2\text{SO}_4/\text{H}_2\text{SO}_4$ reference), temperature and gassing rate vs. time of polarization for sample cell C402, first voltage series VS-1, and $U=2.40V$ [10].

2.3. Integration of Reference Electrodes in VRLA cells for Advanced Battery Management

The immobilisation of the electrolyte in the VRLA cells along with their sealing improved markedly the safety of this system decreasing the possibility for acid spilling or projections in case of an accident. In the same time the traditional method for lead-acid battery diagnostics based on the specific gravity measurement became inapplicable. The kinetics of the oxygen recombination and the mechanism of the thermal runaway phenomenon showed that the voltage regulation during the VRLA battery recharge is no longer a highly reliable charge management strategy. The most logical response to these challenges is the use of reference electrodes as permanently integrated sensors providing additional information about the battery state and the dynamics of the ongoing processes (charge, discharge, floating, open circuit / self-discharge). The electrode couple $\text{Ag}/\text{Ag}_2\text{SO}_4$ in H_2SO_4 was identified by Ruetschi as a promising reference

electrode [11, 12] however with a rather limited lifetime. A major improvement of in terms of smaller size, longer durability and absence of maintenance of the electrode was an object of a patent filed by CEA-LITEN [13]. A scheme of the reference electrode is presented in Figure 2.17a. In the core of this innovation is the immobilisation of the electrolyte in glass-microfiber mat and the compression of the inner electrode assembly by the fitting of the plug of the electrode which also houses the porous junction comprised of graphite with low porosity. The latter is an excellent compromise between the diffusion permeability and ionic contact with the solution of the electrochemical cell and allows the electrode to operate permanently in the lead-acid cell. Figure 2.17b presents a photo of laboratory and industrial prototype reference electrodes which are in use by the team of the Laboratory for Storage of Electricity at CEA-LITEN. The industrial prototype was developed by the French company Material Mates (M^2) during the project CARBOLEAD 2010 financed by ANR.

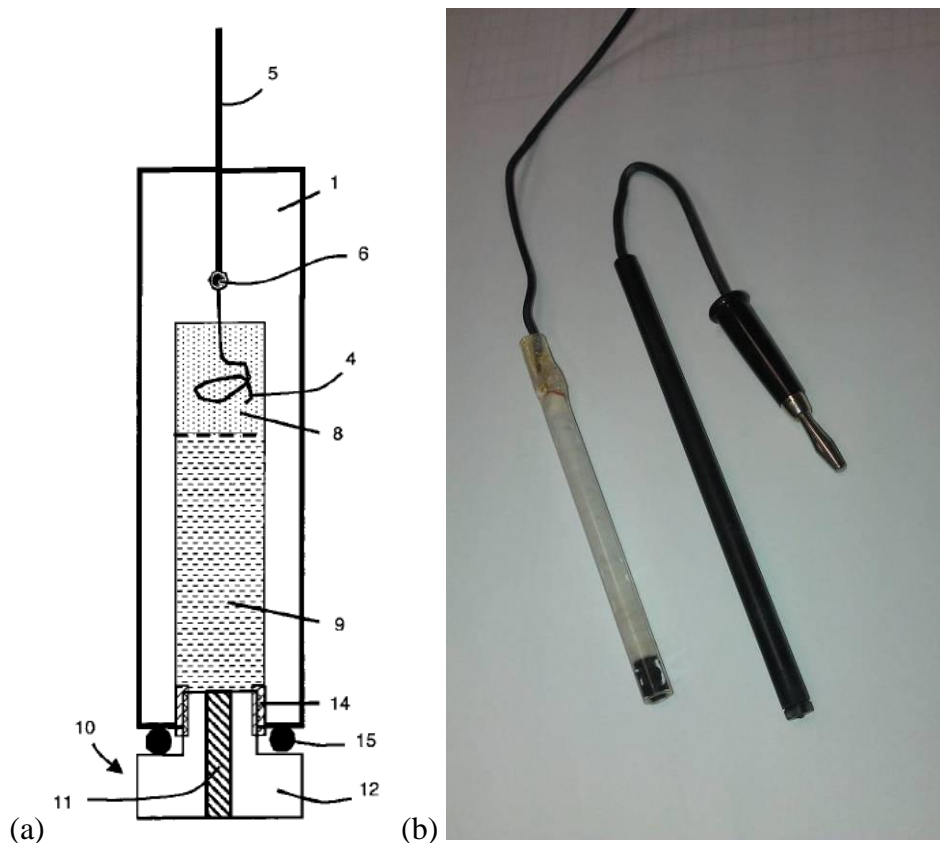


Fig. 2.17. Scheme (a) and photo (b) of $\text{Ag}/\text{Ag}_2\text{SO}_4$ reference electrodes developed in CEA [13].

The splitting of the VRLA cell voltage in positive and negative plate potential allows monitoring and controlling of the phenomena taking place particularly on one of the battery electrode. An example of such strategy can be the State of Charge (SOC) estimation using the negative plate potential at open circuit which was an object of another patent filed by CEA-LITEN [14]. The background beyond the method is presented in Figure 2.18, where the open circuit voltage and half-cell potential transients are plotted in the case of end of charge and end of the discharge of 10Ah flooded cell comprised of one negative and two positive SLI battery plates (STECO Power, France). It can be seen that the cell voltage changes gradually after the interruption of the current making the use of this parameter rather unreliable. The comparison of both half-cell potentials shows that the slow relaxation of the cell voltage is practically

governed by the behaviour of the positive plate. In contrary the negative plate potential reaches a steady state within several minutes making this parameter attractive for a potentiometric estimation of SOC. The dependence of the open circuit negative plate potential as a function of SOC is presented in Figure 2.19. The data show that in addition to the potential measurement, one should take into account the short history of the battery in terms of sign of the current applied prior to SOC estimation due to the appearance of hysteresis effects most probably related to the electrolyte stratification.

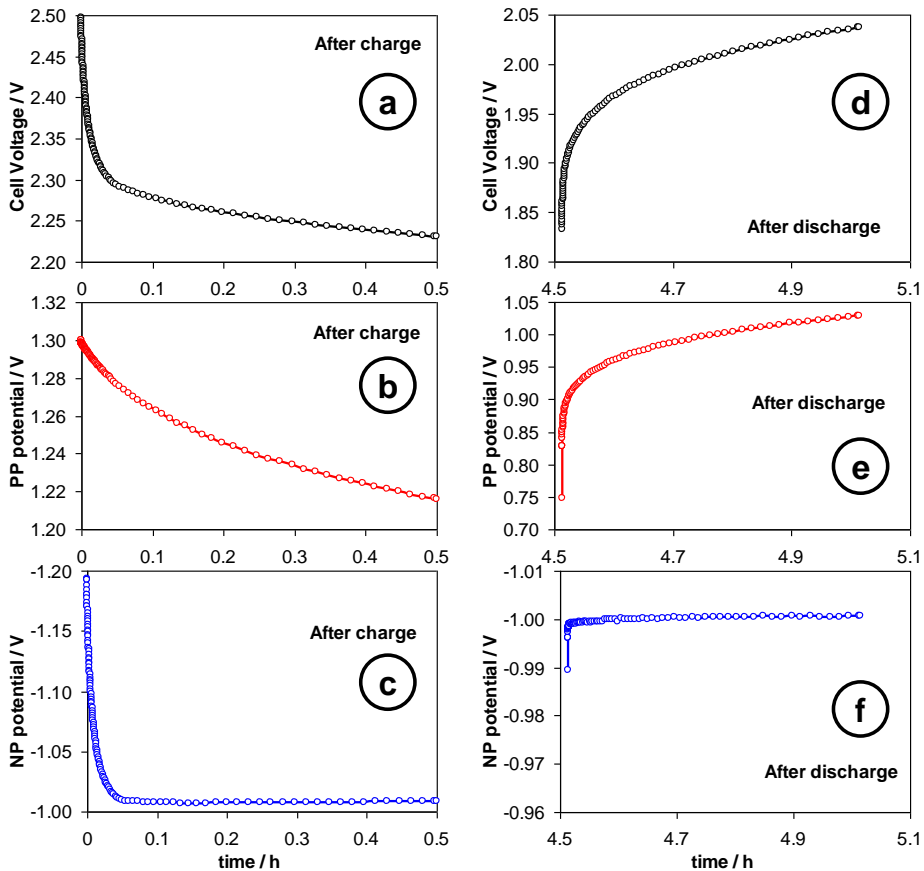


Fig. 2.18. Open circuit transients of the cell voltage, positive and negative plate potential after the interruption of the charge (a, b and c) and the discharge (e, d and f) current [14].

The integrated reference electrodes can be used also in an “active” way in order to control the potential of one of the battery electrodes. A demonstration of such approach was already mentioned in paragraph 2.1. However much more interesting example is the cell or battery recharge controlling the positive plate potential in the end of the charge, i.e. replacing the traditional constant current / constant voltage charge with constant current / constant potential charge. This approach is illustrated in Figure 2.20 for the case of a VRLA cell with one positive and two negative plates equipped with Ag/Ag₂SO₄ reference electrode. The benefit from such charge strategy is the precise control over the process of the oxygen evolution using the positive plate potential. Controlling the oxygen evolution rate, it is possible to limit the rate of the oxygen recombination process and so the heat generated by the oxygen cycle. The latter means that using an integrated reference electrode it is possible to fast charge any VRLA battery without the risk of thermal runaway. Moreover, as it can be seen in Figure 2.20, it is possible to indicate the complete recharge of the negative plates by the inflection point in the transients of the cell voltage and negative plate potential.

The control of the positive plate potential during the charge will also control the rate of the positive grid corrosion [15]. In this way with the use of the reference electrode in the battery management strategy one can increase the battery life substantially. The latter can be particularly efficient in back-up energy storage systems where the battery is at overcharge conditions for most of its life and where the corrosion is usual failure mode [16].

The integrated reference electrode allows also the splitting of the battery impedance into positive and negative plate contribution. The benefits of this approach will be discussed in the next paragraphs.

Fig. 2.19. Experimental dependence of the negative plate potential on SOC after 5min and 1h open circuit stay. The red squares denote the zones where the calibration points should be sampled [14].

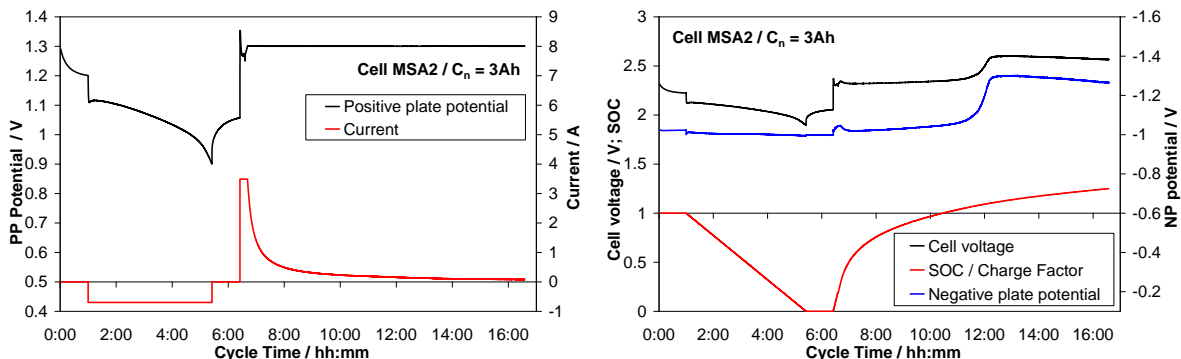
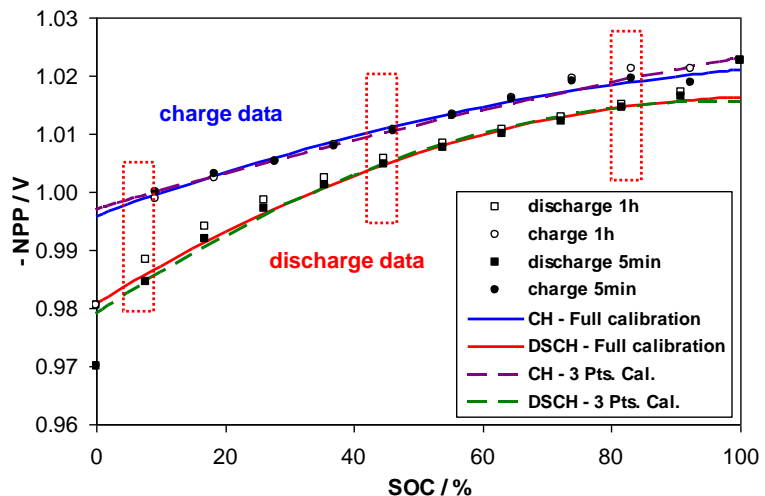


Fig. 2.20. Evolution of the VRLA cell parameters during a cycle with a potential regulated charge and discharge (SOC is normalised using the discharge capacity without further corrections due to side reactions).

2.4. Pulse charge – an interaction between Faradic and capacitive battery properties

One of the usual problems of the VRLA batteries used in cycling and PV (or other renewable) energy applications is the sulfation of the positive and negative plates. This failure mode is often associated with the strict limiting of the charge voltage in the range 2.35-2.40V/cell in order to avoid the battery drying out. Another emerging problem was the application of fast charge algorithms during which the battery should accept high charge currents efficiently. Various separate studies (some done in LSE at CEA-LITEN) indicated that the replacement of the continuous charge current with a pulse current can bring partial or complete solution of the above-mentioned problems associated with the battery sulfation [17, 18].

The replacement of the charge current with pulse current introduce several new parameters for control and monitoring by the Battery Management Systems. This is illustrated in Figure 2.21 for the simple case of “ON/OFF” pulse current, i.e. without pulse reversal sections.

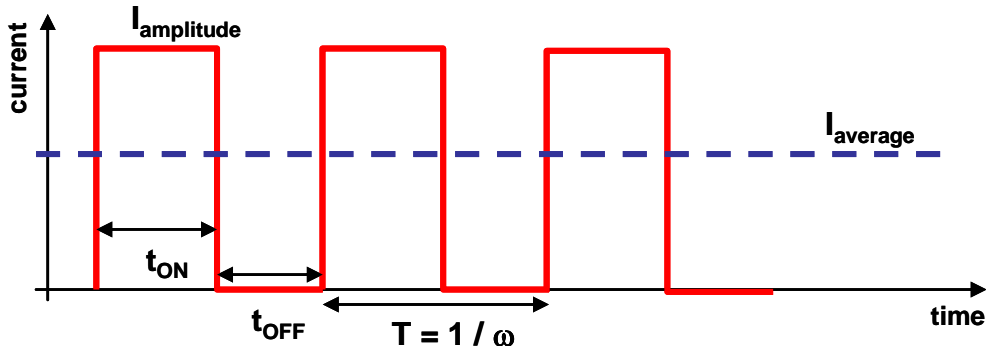


Fig. 2.21. Scheme of a pulse current profile and its characteristic parameters.

The analogue of the continuous current here is the average value of the pulse current:

$$I_{av} = I_{amp} \frac{t_{ON}}{t_{ON} + t_{OFF}} = I_{amp} \cdot r \quad (2.4)$$

Thus for the case of “ON/OFF” type of pulse current there are three variables in terms of amplitude (I_{amp}), pulse cycle ratio (r) and pulse frequency (ω) instead of the simple current rating in the case of continuous battery charging.

The main effect of the pulse current on the battery electrochemistry is the active involvement of the electric double layers (EDL) of both electrodes (positive and negative) in the energy accumulation process. While during the battery charge with continuous current the electric double layer remains always charged, in the case of “ON/OFF” pulse charge the EDL works as a shuttle making a cyclic internal transfer of electrostatic into electrochemical energy storage. In this way the pulse charge is an interaction between Faradic and capacitive battery properties.

The electrochemical impedance spectroscopy is the most suitable method for investigation of the electric double layer in battery electrodes allowing easy separation of the capacitive and Faradic phenomena. Various impedance studies were carried out on model lead-acid cells comprised of positive or negative plate encountered by a pair of counter-plates with the same or larger size and a reference electrode. Such a configuration ensures a symmetric and homogeneous distribution of the electric field at both sides of the working electrode and delivers optimal conditions for impedance measurements.

The impedance was analyzed using two complementary strategies – electric equivalent circuits (EEC) approach and differential impedance analysis (DIA). The latter was developed by Stoynov as a method for impedance data analysis delivering information about the studied object without a proposal of preliminary hypothesis about the model of the system [19]. In brief, DIA gives information about the number and the magnitude of time constants, resistive, capacitive and distributed elements in the studied AC frequency domain. This information can be used further in the finding of the most realistic equivalent circuit model for data fitting and parameter extraction.

In order to link efficiently the impedance data with the physics of the studied system, one has to be able to change the system state in a known way, measuring its response in terms of impedance spectra evolution. In the classic electrochemistry under isothermal conditions the

change of the system state is usually carried out by change of the electrode potential. Such kind of operating mode is hardly possible when porous battery electrodes are studied (some exceptions will be discussed too) due to the huge magnitudes of the current response. In this case the change of the potential is replaced by the change of the State of Charge. The latter represents the ratio between the available and the total electrode capacity for reversible storage of electricity.

2.4.1. Impedance of the positive plate

The impedance spectrum of partially charged 8Ah positive plate (pasted technology with Pb-2.8%Sb grid) is presented in Figure 2.22 together with the results from the differential impedance analysis [20]. Both the Nyquist plot and DIA data (in terms of frequency distribution of the Local Operating Model parameters) indicate the presence of three time constants as well as the beginning of a diffusion tail. The combination of these data with the gel-crystal model of the PbO₂/PbSO₄/H₂SO₄ electrode proposed by Pavlov led to the electric equivalent circuit of the positive plate presented in Figure 2.23. The presence of a pseudo-inductive loop at high frequencies indicates the presence of fast chemical reactions involved in the hydration / dehydration (crystallization) of the lead dioxide. The high frequency capacitive loop can be related to the mixed conductivity of the hydrated layer on the surface of the positive active material. The third time constant found at lower frequencies can be related to the charge transfer resistance and EDL capacitance. The impedance spectrum calculated from the fit parameters was also subjected to DIA and put in Figure 2.22b as solid curves. The observed good correlation between the measured and simulated DIA data supports additionally the proposed equivalent circuit. The application of the equivalent circuit approach allowed obtaining the values of EDL capacitance as a function of SOC. Figure 2.24 presents the corresponding results. Surprisingly, there is a very well pronounced hysteresis which is fairly reproducible both from cell to cell as well as at different ageing states (cycle number). Such a result can be explained only by substantial changes of EDL structure linked strongly with the electrochemical processes of charge and discharge. The latter is illustrated in Fig. 2.25. During the charge process the water is consumed to form hydrated PbO(OH)₂ with HSO₄⁻ anions adsorbed on its surface. In this case EDL can be represented as a simple capacitor with corresponding thickness, dielectric constant and surface charge density. During the overcharge the water is decomposed and the formed H⁺ are first incorporated in the Stern layer decreasing the effective surface charge density which explains the rapid decrease of EDL capacitance. During the discharge, water molecules are formed locally between the PbO₂ surface and the Stern layer leading to EDL with a structure similar to those on metals. Such a structure corresponds to EDL capacitance 6-7 times lower in comparison with the one during the charge at the same specific surface area (respectively same SOC value). The high values of EDL capacitance on the positive plate (up to 150F/Ah) demonstrate that this electrode has remarkable super-cap properties. This explains the good performance of the positive plates under High Rate Partial State of Charge (HRPSOC) cycling conditions where high charge appendance of short charge pulses is necessary.

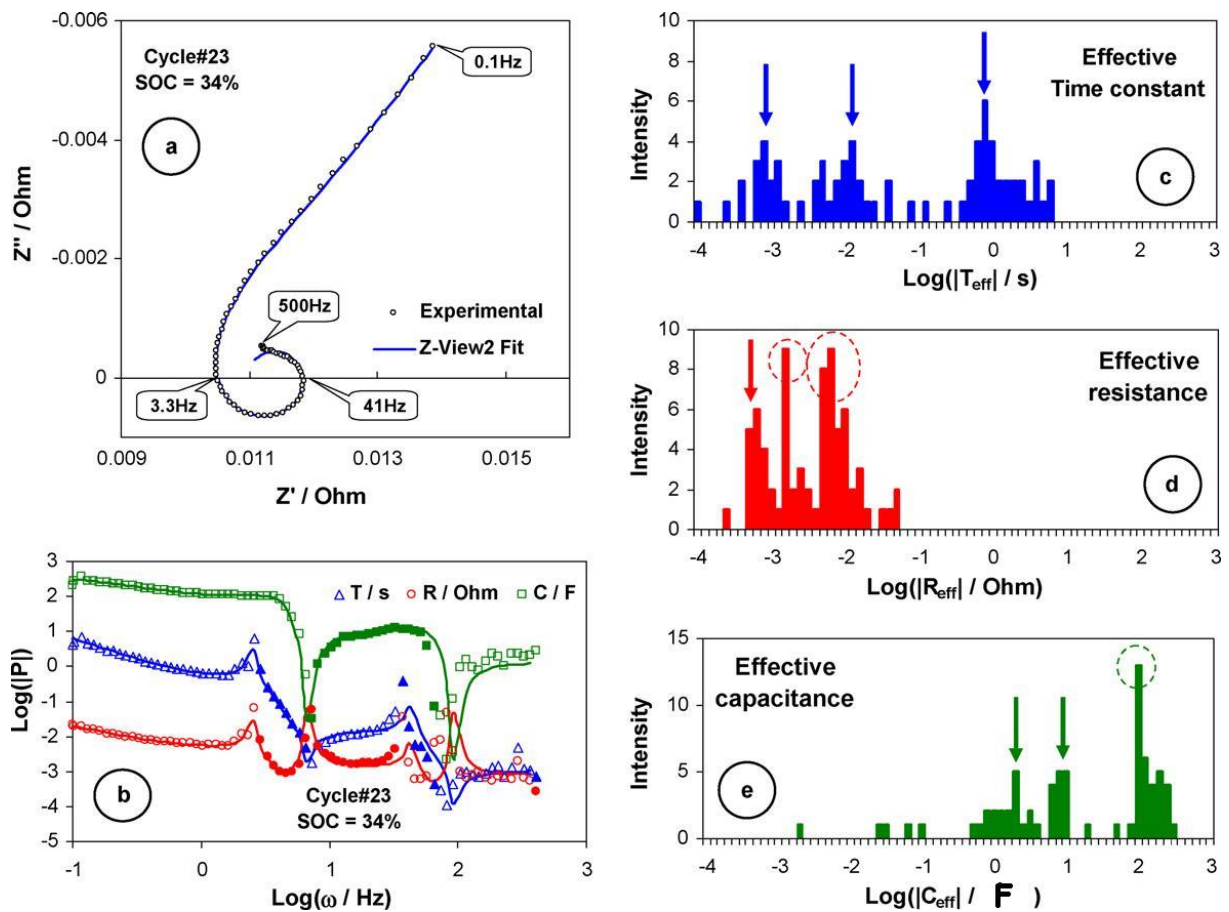


Fig. 2.22. (a) Electrochemical impedance spectrum of a partially charged positive plate after 23 charge/discharge cycles in 1.24 s.g. electrolyte, SOC = 34%. (b) Differential impedance analysis temporal plot representation of the impedance spectrum, the white-filled symbols correspond to positive values of the LOM parameters, the colour-filled symbols correspond to negative values of the LOM parameters, the solid lines correspond to the DIA of the simulated EIS with the circuit parameters form the best fit. (c-e) Spectral DIA plots of the LOM parameters, the units of the intensity are in number of points per spectral line, the spectral density is 10 points per decade [20].

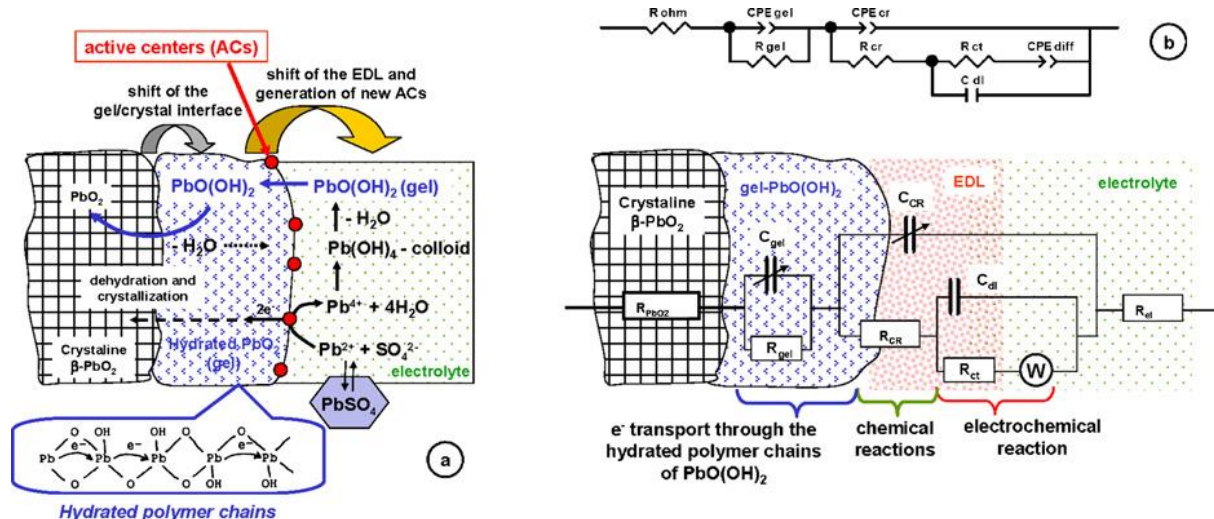


Fig. 2.23. Scheme of the PbO₂/electrolyte interface, the reactions taking place there (a) and their equivalent circuit representation during the charge of the positive plate (b) [20].

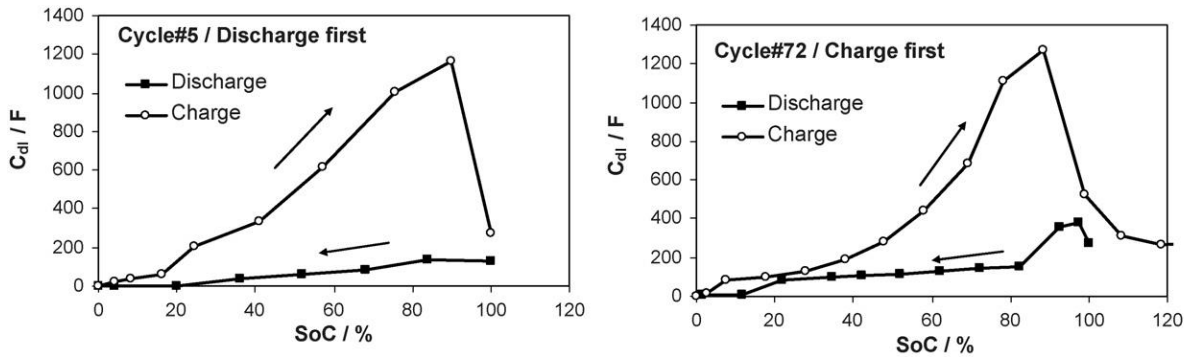


Fig. 2.24. Dependence of the EDL capacitance C_{dl} on state of charge for a cell (8Ah positive plate) subjected to 5 cycles and for a cell subjected to 72 cycles with 100% DOD at 10 h rate of the charge and the discharge (0.8 A) [20].

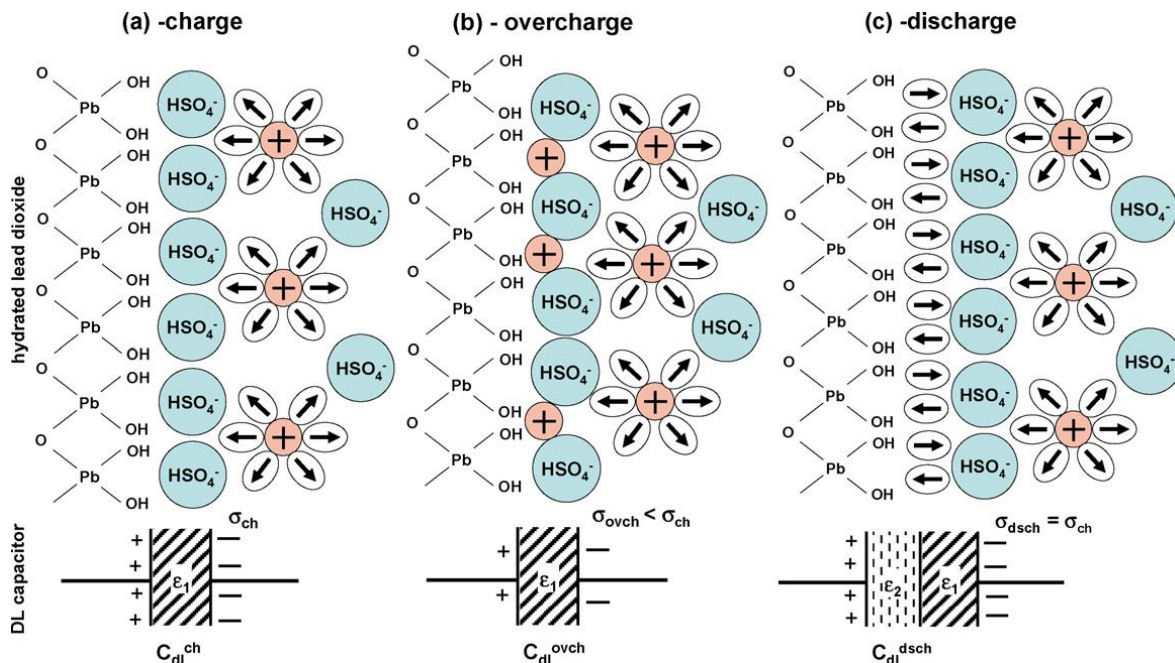


Fig. 2.25. Model of the EDL on the surface of the hydrated lead dioxide during the charge (a), the overcharge (b) and the discharge (c). The surface density of the charges (Cm^{-2}) is denoted as σ_{ch} , σ_{ovch} and σ_{dsch} for the charge, the overcharge and the discharge. The water dipoles are denoted with arrows and the H^+ ions with “+” [20].

2.4.2. Impedance of the negative plate

The impedance of the negative plate is the key moment in the understanding of the lead-acid battery operation at HRPSOC cycling. This type of cycling is one of the very few cases where the negative plate is the reason of the lead-acid battery failure. The usual strategy for overcoming this problem is the addition of different type of carbons, often with high specific surface area [21]. Here, the impedance spectroscopy offers fast and comprehensive way to evaluate the impact of the carbon addition in terms of improvement of the resistance components (R_Ω and R_{ct}) and double layer contribution.

Figure 2.26 presents the evolution of the negative plate impedance during the charge, together with the results from the differential impedance analysis. The results from DIA indicate three

frequency domains with distributed time constants. The frequency dependence of the local capacitance (C_{eff}) shows that the capacitive elements in all three domains have constant phase element behaviour. The high frequency time constant can be related to the main electrochemical process on the negative plate – the conversion of the lead sulphate into lead.

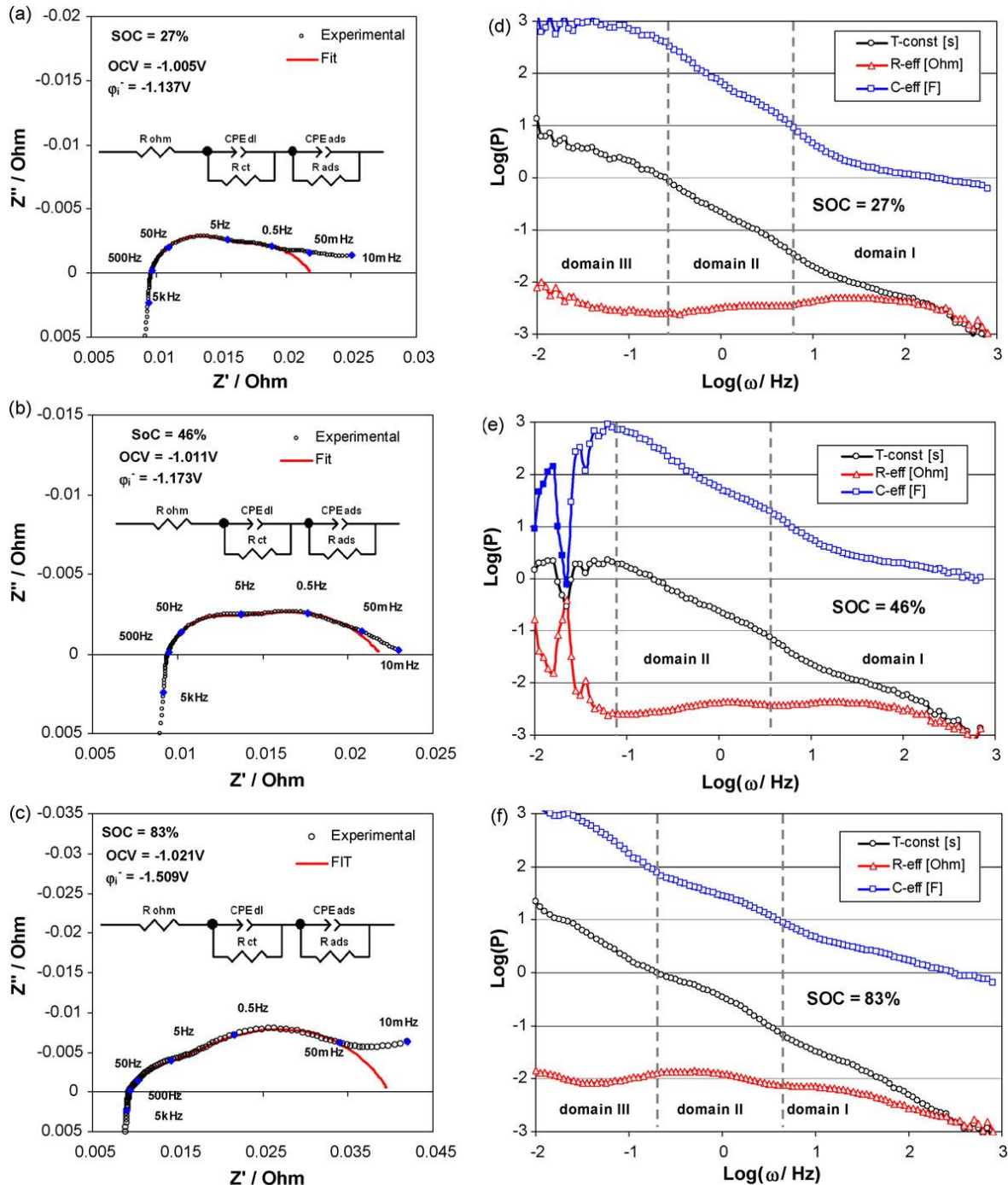


Fig. 2.26. Evolution of the negative plate impedance during the pulse charge of 9Ah flooded cell (two positive plates vs. one negative and Ag/Ag₂SO₄ reference [22].

The medium frequency time constant can be related to the adsorption of the expander molecules on the surface of the lead crystals. The low frequency time constant is more complex, being capacitive or pseudo-inductive depending on SOC and the polarisation history. In some cases it is often rather hard to be recognised clearly. Considering the pulse charge and HRPSOC

cycling topics, it is interesting to analyse only the first two frequency domains because they include the most important rate-limiting steps.

The evolution of the negative plate equivalent circuit parameters with SOC is presented in Figure 2.27. The constant phase elements were converted in capacitance values using the methodology proposed by Hsu and Mansfeld [23]. It can be seen that for 9Ah plate with NAM utilisation ~50% the double layer capacitance at SOC = 100% is about 7F. Considering a typical specific surface area of $0.5\text{m}^2/\text{g}$, the specific capacitance of the negative plate is about $20\mu\text{F}/\text{cm}^2$ which is fairly close to the measurements of EDL capacitance on smooth lead electrodes in H_2SO_4 [24]. The latter demonstrates well the adequacy of the equivalent circuit approach on porous lead-acid battery electrodes, both positive and negative, at least in the frequency domain down to about 10mHz.

All four equivalent circuit parameters show a well pronounced hysteresis when plotted as a function of SOC. This hysteresis can be explained by the dynamics of the adsorption of the expander (usually lignosulfonate macromolecules). During the electrode charge when lead is electrodeposited the expander molecules are adsorbed on the electrode surface acting as membrane with reduced ion permeability, which limits the charge acceptance of high current peaks. When the electrode is discharged the lead dissolves leading to desorption of the expander and increased lead (II) ion concentration in the close proximity of the lead metal surface. The latter decreases the charge transfer resistance and increases the double layer capacitance since the latter is proportional to the surface density of the charges.

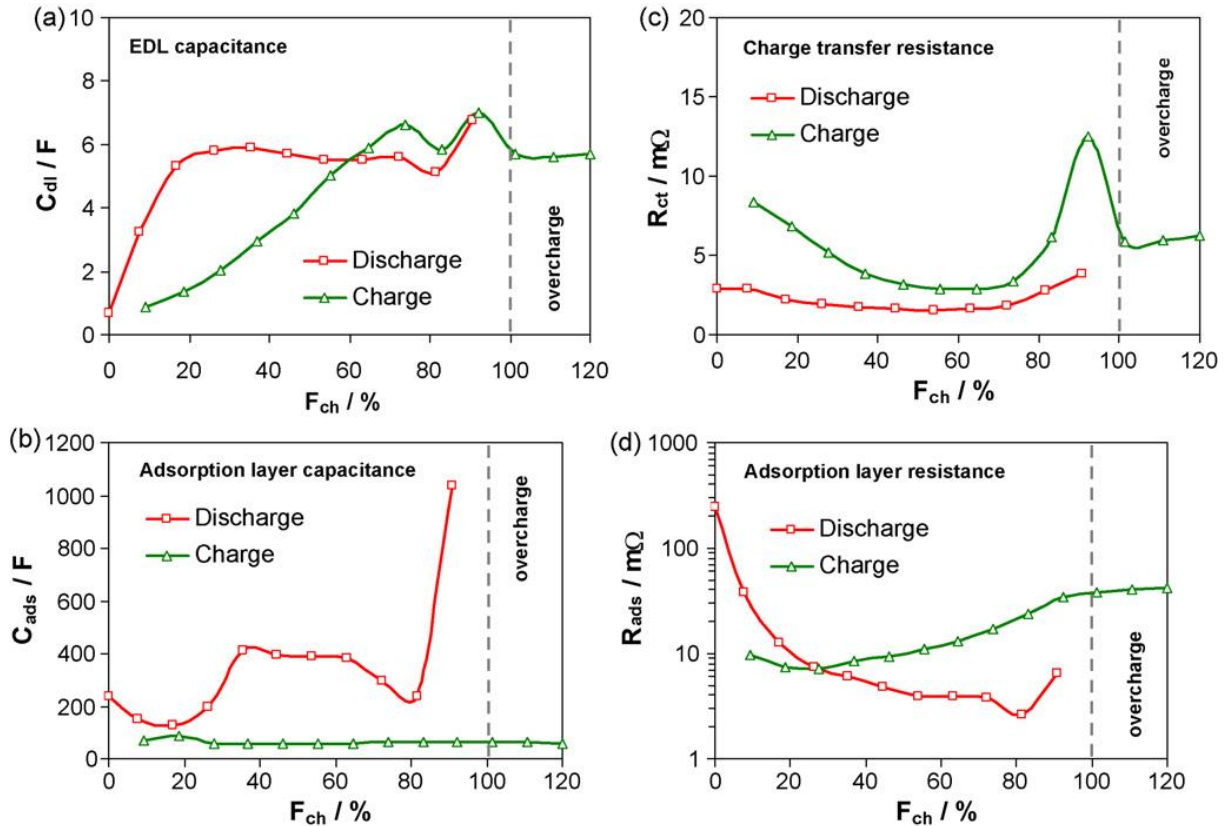


Fig. 2.27. Dependence of EDL capacitance (a), charge transfer resistance (b), adsorption capacitance (c) and adsorption resistance (d) on the quantity of the injected charge expressed as a charge factor. The data are for 9 Ah flooded cell [22].

Here it is particularly interesting to compare the capacitance of EDL on the positive and on the negative plate (Figure 2.23 and 2.27a). It can be seen that for the nearly same Ah capacity the double layer capacitance of the positive plate is between 10 and 100 time higher. This huge difference comes from the difference in the specific surface area of the materials ($5\text{m}^2/\text{g}$ for PAM and $0.5\text{m}^2/\text{g}$ for NAM). Considering the pulse charge, it means that the positive plate would favour pulse profiles with smaller pulse cycle ratio and higher amplitude while the negative plate would “prefer” pulses with lower amplitudes and higher pulse cycle ratio.

2.4.3. Electrochemical resonance

In the course of the pulse charge studies carried out in LSE it was necessary to quantify the involvement of the double layer in the electrochemical processes during the pulse charge. Thus, the parameter “average double layer current” was introduced [25]. In the case of positive plate, the double layer current is proportional to the capacitance of EDL and the derivative of the electrode potential

$$I_{DL} = C_{DL} \frac{d\varphi^+}{dt} \quad (2.5)$$

For a pulse current with pulse cycle ratio $r = 0.5$ ($t_{ON} = t_{OFF}$) the average double layer current can be expressed as

$$\langle I_{DL} \rangle = 2\omega \int_0^{1/2\omega} I_{DL} dt = 2\omega C_{DL} (\varphi_{end}^+ - \varphi_0^+) \quad (2.6)$$

where φ_0^+ and φ_{end}^+ are the positive plate potential values in the beginning and in the end of the “ON” or “OFF” half-period as it is illustrated in Figure 2.28. It is important to note that the value of φ_0^+ should be accounted excluding the effect of the ohmic drop IR_{int} due to the internal resistance of the cell. The average double layer current is rather simple to derive parameter knowing the value of EDL capacitance in the moment of the pulse charge application (i.e. at the given SOC value).

Fig. 2.28. Positive plate potential transient in the beginning of the pulse charge period starting after galvanostatic charge of 8Ah positive plate with $C/10h$ rated current up to 1.4V vs. $\text{Ag}/\text{Ag}_2\text{SO}_4$ [25].

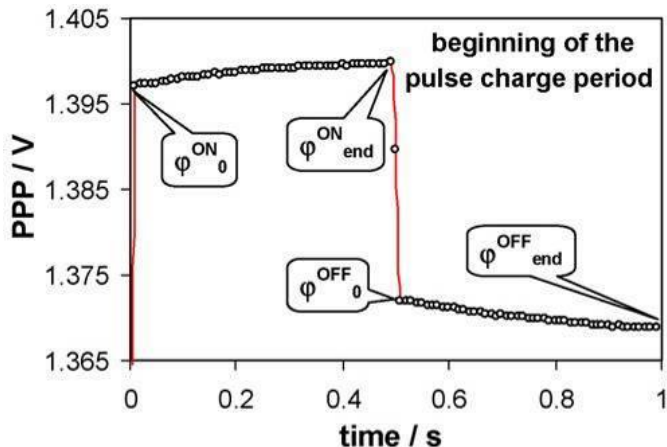


Figure 2.29 plots the dependence of the average double layer current on the pulse charge frequency for the case of 8Ah positive plate. It can be seen that there is a well pronounced maximum at 1Hz. The impedance measurements performed in the same SOC range give a charge transfer resistance values around 2mOhm and EDL capacitance about 300-400F. The characteristic frequency of a parallel RC circuit which represents a simple Faradic process is proportional to the $1/(R_{ct}C_{DL})$. Thus, using the impedance spectroscopy data one obtains a

characteristic frequency values fairly close to 1Hz. The studies of Benchetrite [17] and Karoui [18] carried out in CEA-LITEN concluded that the same frequency of the pulse charge is very beneficial for the battery lifetime in terms of both capacity and water loss.

In the physics, when a given system is perturbed with a periodic oscillation with a frequency close to its characteristic frequency, it starts absorbing the energy of the applied perturbation with maximum efficiency. The phenomenon is denoted as resonance and it occurs both in very small objects on quantum level up to very big objects like musical instruments.

Thus the recharge of a battery electrode with a pulse current having a frequency close to its characteristic frequency, i.e. $1/(R_{ct}C_{DL})$, can be denoted as “electrochemical resonance”. At the resonance conditions the electrode should absorb the energy in the most efficient way, which means that the charge acceptance will be maximal.

Fig. 2.29. Average double layer current as a function of the pulse current frequency (beginning of the pulse charge at 1.4V vs. SSE, end of the charge 3h later). Capacity of the cell 8Ah, pulse current amplitude 0.8A, pulse cycle ration $r = 0.5$ [25].

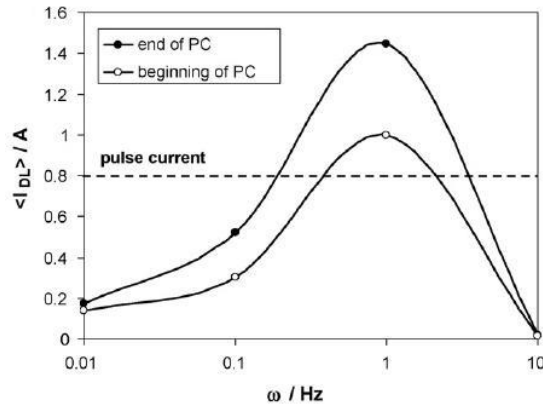


Figure 2.30 presents the characteristic frequency $(R_{ct}C_{DL})^{-1}$ of the negative plates of 10Ah gel VRLA cell as a function of the charge factor (ratio between injected charge and the previously obtained discharge capacity). It can be seen that the lower capacitance of EDL on the negative plate results in considerably higher characteristic frequencies. The relationship between the pulse current frequency and the charge acceptance is further illustrated in Figure 2.31, where a 10Ah gel-VRLA cell is subjected to a series of charge current pulses with amplitude equal to 2A and pulse cycle ratio $r = 0.5$, i.e. keeping same average charge current. It can be seen how increasing the pulse current frequency the negative plate polarisation decreases indicating improving charge acceptance.

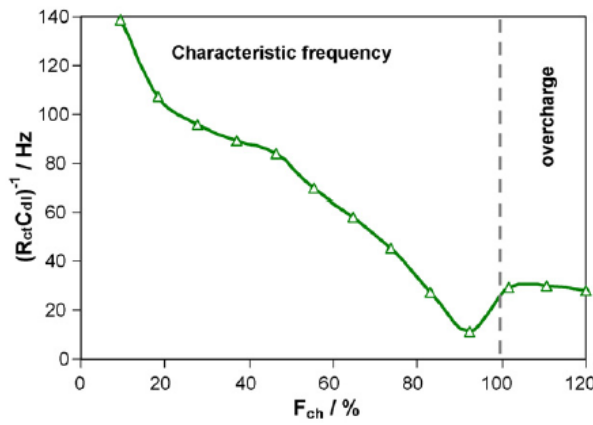


Fig. 2.30. Dependence of the characteristic frequency of the $PbSO_4$ reduction process on the quantity of the injected charge [22].

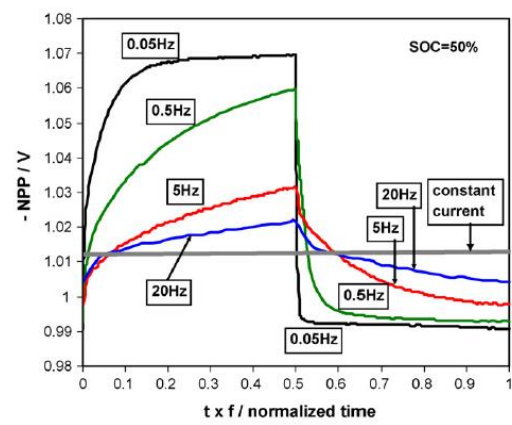


Fig. 2.31. Negative plate potential transients at SOC = 50% measured during charge of 10Ah gel-VRLA cell, with pulse current with amplitude of 2A [22].

The separate studies of the pulse charge mechanism on the positive and on the negative plate show that this kind of battery management strategy could be used to resolve some particular issues. For deep cycle and solar batteries, these issues are related to the performance of the positive plates requiring pulse charge with frequency around 1Hz. For batteries operating at HRPSOC where the negative plates limit the charge acceptance of the battery, it is necessary to use pulse current with considerably higher frequency 50-100Hz or more.

Chapter 3

Components for Advanced Valve-Regulated Lead Acid Batteries

3.1. The electrolyte as the third active material

The sulphuric acid electrolyte holds a special position in the lead-acid battery electrochemistry – from one hand it is the ionic conductor in the system, from the other it works as an active material being depleted during the discharge. The half-cell electrochemical reactions on the positive and the negative plate



suggest that the lead dioxide electrode will be much more susceptible to electrolyte concentration effects because each bisulphate anion is replaced by two water molecules. Moreover the lead dioxide reacts with the water forming hydrated structures which impact PAM performance like active material utilisation and ageing rate in terms of softening and shedding [26]. The sulphuric acid concentration exerts a strong effect on the lead sulphate solubility. The latter changes from 1mg/l in completely charged state up to about 6mg/l for deeply discharged batteries designed for high utilisation of the electrolyte [27].

There are some considerable differences in the electrolyte concentration depending on the design and the application of the battery:

- The electrolyte concentration in the flooded lead-acid batteries for SLI (starting, lighting and ignition of gasoline and diesel engine vehicles) applications corresponds to a specific gravity of 1.28g/ml (37% / 4.9M). This concentration is close to the minimum in the freezing point diagram of the aqueous sulphuric acid (~ -70°C) as well as to its maximum conductivity.
- The electrolyte in the flooded tubular batteries corresponds to a specific gravity of about 1.24g/ml (33% / 4.2M). It was hard to find bibliographic references discussing this particular choice.
- The electrolyte in the AGM-VRLA batteries often reaches specific gravity values up to 1.30-1.31g/ml (41% / 5.5M) when thinner separators are used in order to achieve lower internal resistance and higher specific energy values.

The last two types of batteries are used both in deep cycling and partial state of charge cycling applications. In addition the positive active material is microporous system making the local variations of the electrolyte concentration on cycling even more extreme.

3.1.1. The Pb/PbO₂/PbSO₄/H₂SO₄ electrode system

The effects of the electrolyte concentration on the Pb/PbO₂/PbSO₄/H₂SO₄ electrode system was studied using Planté-type electrode comprised of lead slab electrodes (99.999% Pb) with geometric surface of about 4cm². The electrodes were cycled in three-electrode system equipped with Pt counter-electrode and Hg/Hg₂SO₄ reference electrode filled with H₂SO₄ with concentration same as the one in the electrochemical cell [28, 29]. The electrode structure was formed applying continuous linear sweep voltammetric cycling between 0.7 and 1.6V with a rate of 100mV/s. Under these conditions the surface of the electrode develops a structure with highly developed porosity similar to the so-called Planté positive plates. The surface morphology of such structure resembles a positive active material operating at the given electrolyte concentration as well as the interface region between the active material and the corrosion layer. The electrodes were cycled for 1h (200 cycles) and 16h (3200 cycles) in order to distinguish short-term and long-term cycle effects. The cyclic voltammograms after 3200 cycles in several different electrolytes are presented in Figure 3.1.

In 5M H₂SO₄ electrolyte the peak C₁ is well pronounced. The reduction is fast and rather small portions of lead dioxide are accumulated in the anodic layer on cycling. In more diluted electrolyte the reduction of the lead dioxide occurs at more negative potentials. Hence larger amounts of it are accumulated on cycling. In general the shape of the voltammograms undergoes an evolution with the change of the electrolyte concentration.

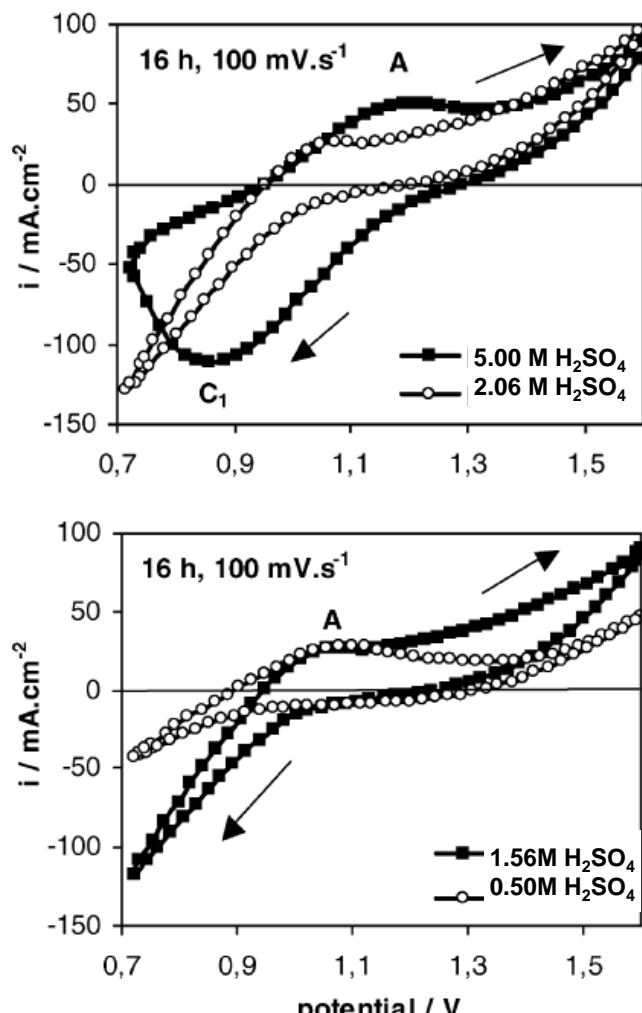


Fig. 3.1. Voltammograms for electrodes cycled at a scan rate of 100mV/s for 16h in various H₂SO₄ electrolytes [28].

Figure 3.2 presents the dependence of the electrode capacity and phase composition of the Planté electrodes removed from the cell at 1600mV. The latter was derived by X-ray diffraction analysis of the surface of the lead slab after washing and drying.

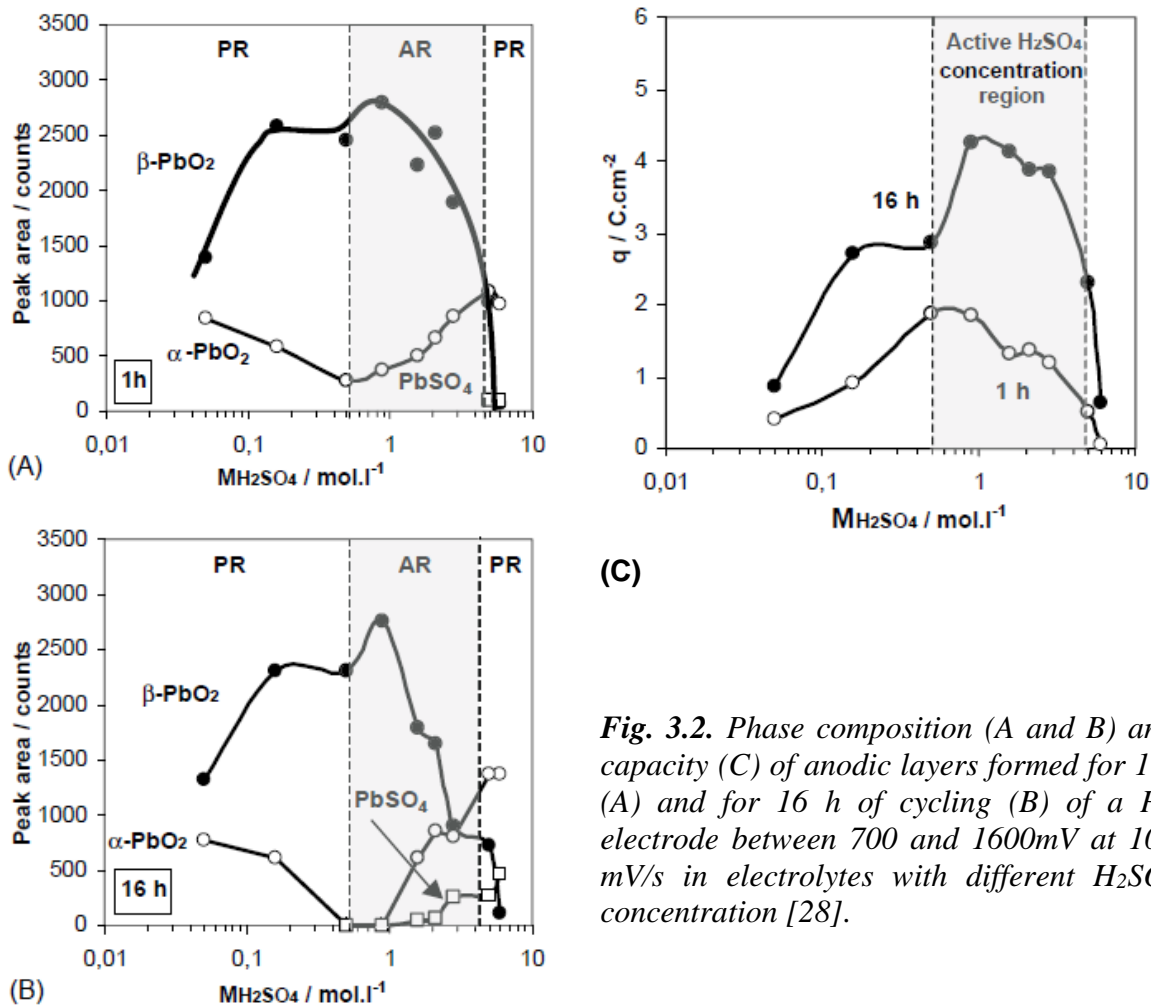


Fig. 3.2. Phase composition (A and B) and capacity (C) of anodic layers formed for 1 h (A) and for 16 h of cycling (B) of a Pb electrode between 700 and 1600mV at 100 mV/s in electrolytes with different H_2SO_4 concentration [28].

The results are rather curious – there is a region of H_2SO_4 concentration with maximum of the electrode capacity indicating a thicker Planté layer. In the very maximum point the phase composition is comprised exclusively of $\beta\text{-PbO}_2$. Moving far from this maximum, the thickness of the layer decreases and so do the ratio β/α PbO_2 . Additionally in the acid concentration region 0.5 – 1.5M it was observed intensive particle detachment (shedding) being most intensive in 0.5M H_2SO_4 electrolyte. This concentration region coincides well with the maximum of the PbSO_4 solubility and was denoted as “active region”. The electrolyte concentration outside the “active region” was denoted as “passive region”. The electrolyte concentration region between 4M and 5M H_2SO_4 is particularly interesting from the battery point of view because it appears that the increase of the concentration shifts the processes from the “precipitation/dissolution” mechanism typical for the positive active mass towards grid corrosion where the lead metal is oxidized to $\alpha\text{-PbO}_2$ via solid state mechanism with oxygen species insertion.

Figure 3.3 presents SEM micrographs of the surface of the anodic layer in 1.58M H_2SO_4 in “charged state” (electrode extracted from the cell at 1600mV vs. MSE). The low and medium magnifications (Fig. 3.3a and 3.3b) indicate the presence of rhombic crystal formations. However at higher magnifications it becomes visible that these are self-assembled structures of

β -PbO₂ nano-particles retaining the shape of the PbSO₄ crystals. The existence of such large agglomerates results in porous layer with enhanced electrolyte access.

In contrast the anodic layer formed in 6M H₂SO₄ and presented in Figure 3.4 features very dense structure formed by compactly arranged larger α -PbO₂ nano-particles with small amounts of β -PbO₂ and PbSO₄ which remains unoxidized at 1600mV vs. MSE.

The results observed on positive “Planté” electrodes showed that the sulphuric acid concentration can influence strongly the PbO₂/PbSO₄ electrode system and the positive plate itself. H₂SO₄ concentration levels above 5M may induce passivation-like phenomena, which can limit the active mass utilization and shorten the cycle life of the battery [30].

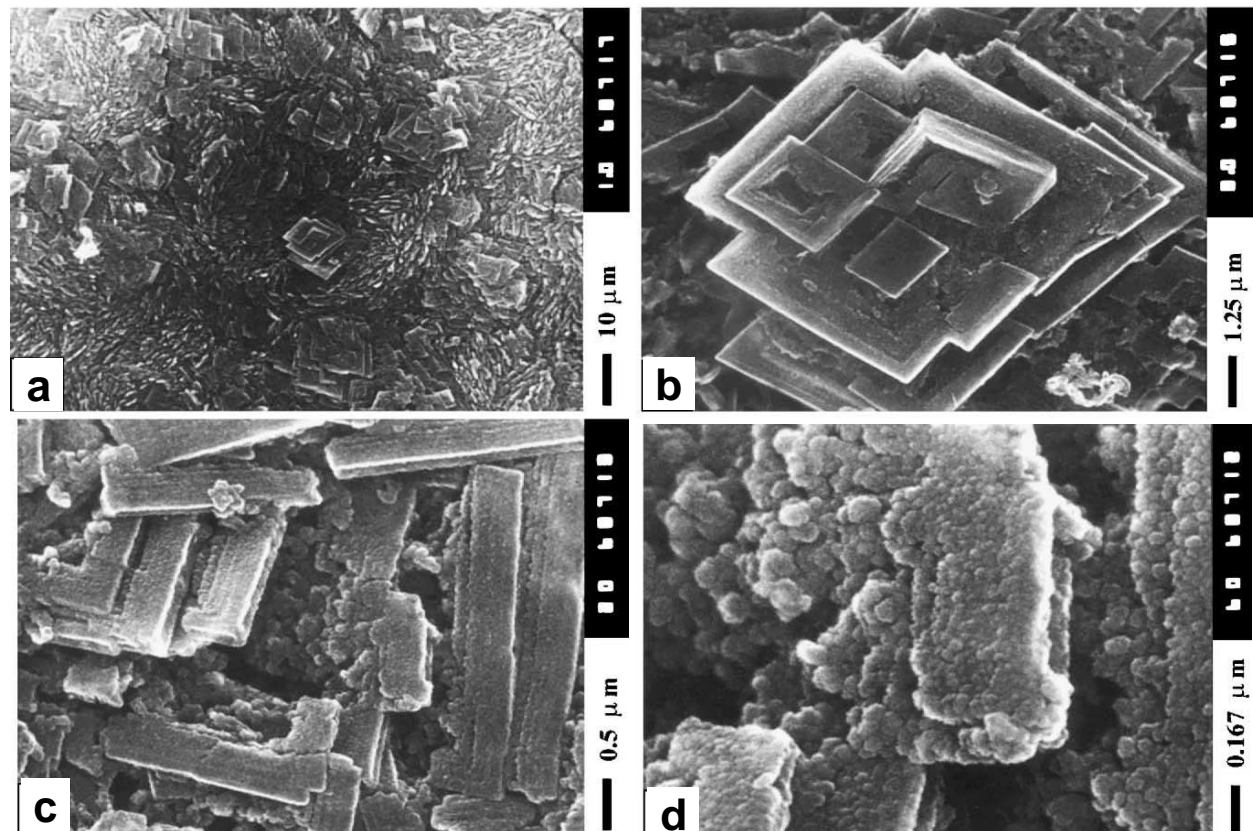


Fig. 3.3. Structure of the anodic layer formed after 1 h of cycling of a Pb/PbO₂/PbSO₄ electrode in 1.58M H₂SO₄ solution [29].

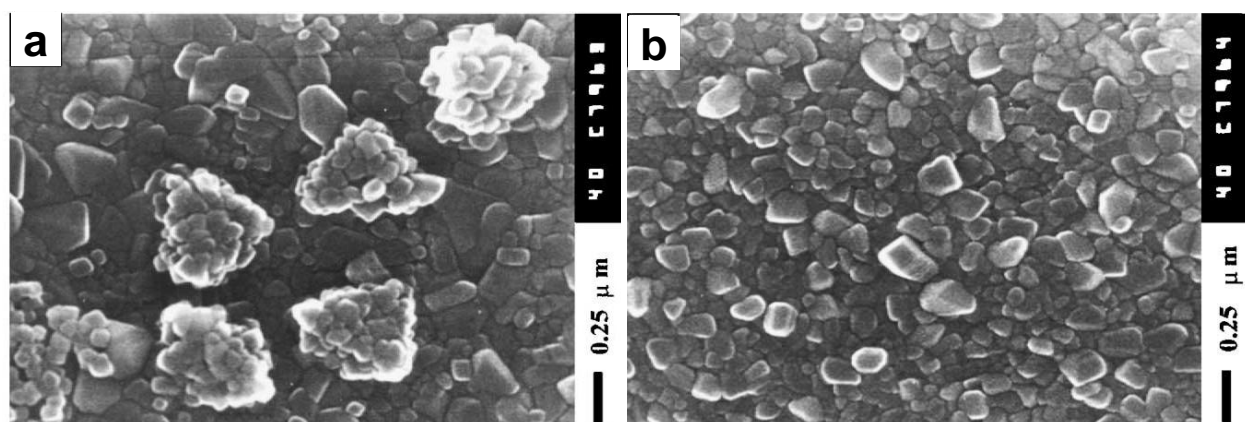


Fig. 3.4. Structure of the anodic layer formed after 1 h of cycling of a Pb/PbO₂/PbSO₄ electrode in 6M H₂SO₄ solution. Electrode polarization was stopped at 1600mV [29].

3.1.2. Influence of the sulphuric acid concentration on the positive plate performance

The impact of the electrolyte concentration on the positive plate performance and electrochemistry was further studied in CEA-LSE using cells similar to the ones described in 2.4.1 comprised of 3Ah traction positive plate encountered by a pair of negative plates with similar size (~3Ah) [31]. Figure 3.5 presents the positive plate potential discharge transients in different electrolytes at 6h-rated current (0.5A) as well as the resulting capacity vs. electrolyte concentration dependence. It can be seen that between 3M and 4.5M H₂SO₄ (s.g. 1.15 - 1.26g/ml) the utilisation of PAM is optimal with a maximum at about 4M H₂SO₄ (s.g. ~1.24). Decreasing the acid concentration (at SOC = 100%) below 3M results in gradual decrease of the capacity following the curve of the Amp-hour equivalent of the electrolyte in the cell. The obtained results indicate that for a maximal utilisation of PAM the battery design should include no more than 50-55% utilisation of the electrolyte. The sulphuric acid concentration in the end of the discharge is in the range of 1.5-2mol/l (s.g. ~1.10-1.12g/ml).

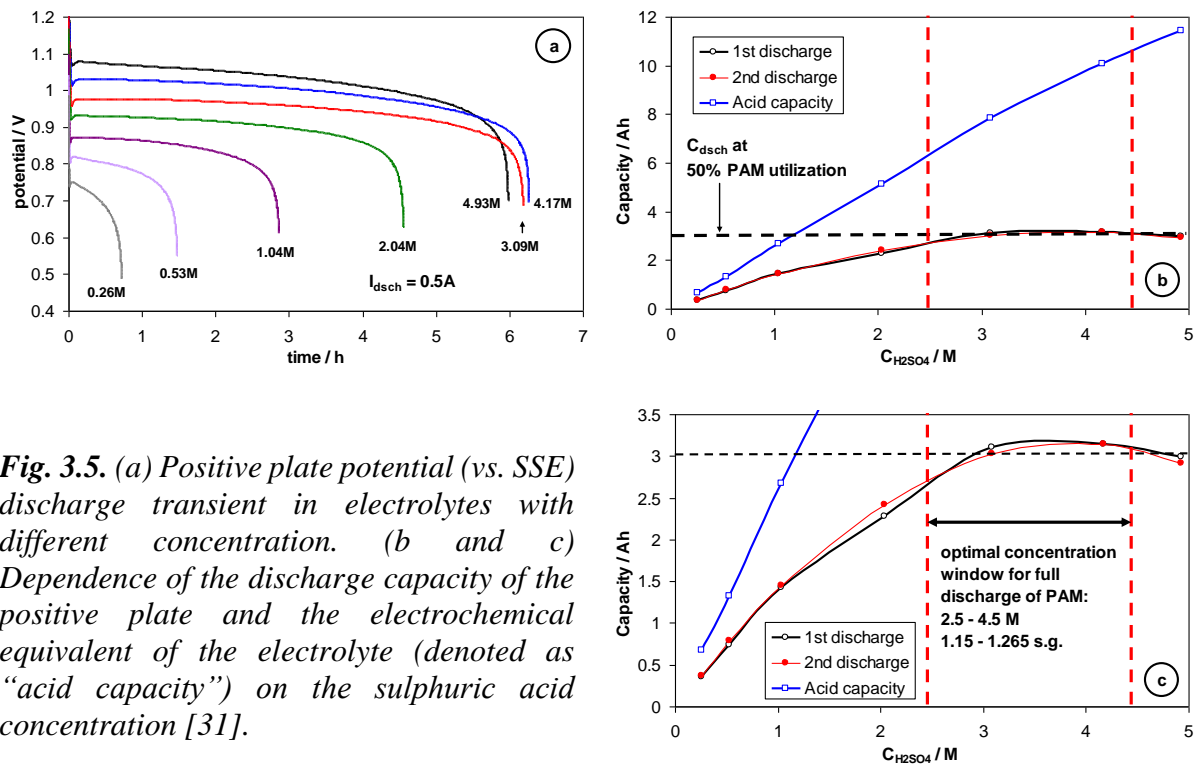


Fig. 3.5. (a) Positive plate potential (vs. SSE) discharge transient in electrolytes with different concentration. (b) and (c) Dependence of the discharge capacity of the positive plate and the electrochemical equivalent of the electrolyte (denoted as “acid capacity”) on the sulphuric acid concentration [31].

The concentration of the electrolyte influences the charge process in two aspects: from one hand when the concentration of the sulphuric acid increases, the solubility of the lead sulphate decreases and so does the charge acceptance. From the other hand, the electrolyte concentration may change the oxygen evolution kinetics. Figure 3.6 presents Tafel plots of the oxygen evolution current in a completely charged cell from the type mentioned above. It can be seen that the electrolyte concentration exerts quite dramatic effect on the oxygen overvoltage. The Tafel coefficient “b” increases slightly from 90 to 100mV/dec in more concentrated electrolyte indicating minor changes in the mechanism of the process. The increase of the coefficient “a” is much greater supposing a considerable decrease in the number of active sites for oxygen evolution in more concentrated sulphuric acid. The effect can be quantified in terms of concentration coefficient of the oxygen evolution being about 15mV/M, where M indicates the molarity of the electrolyte.

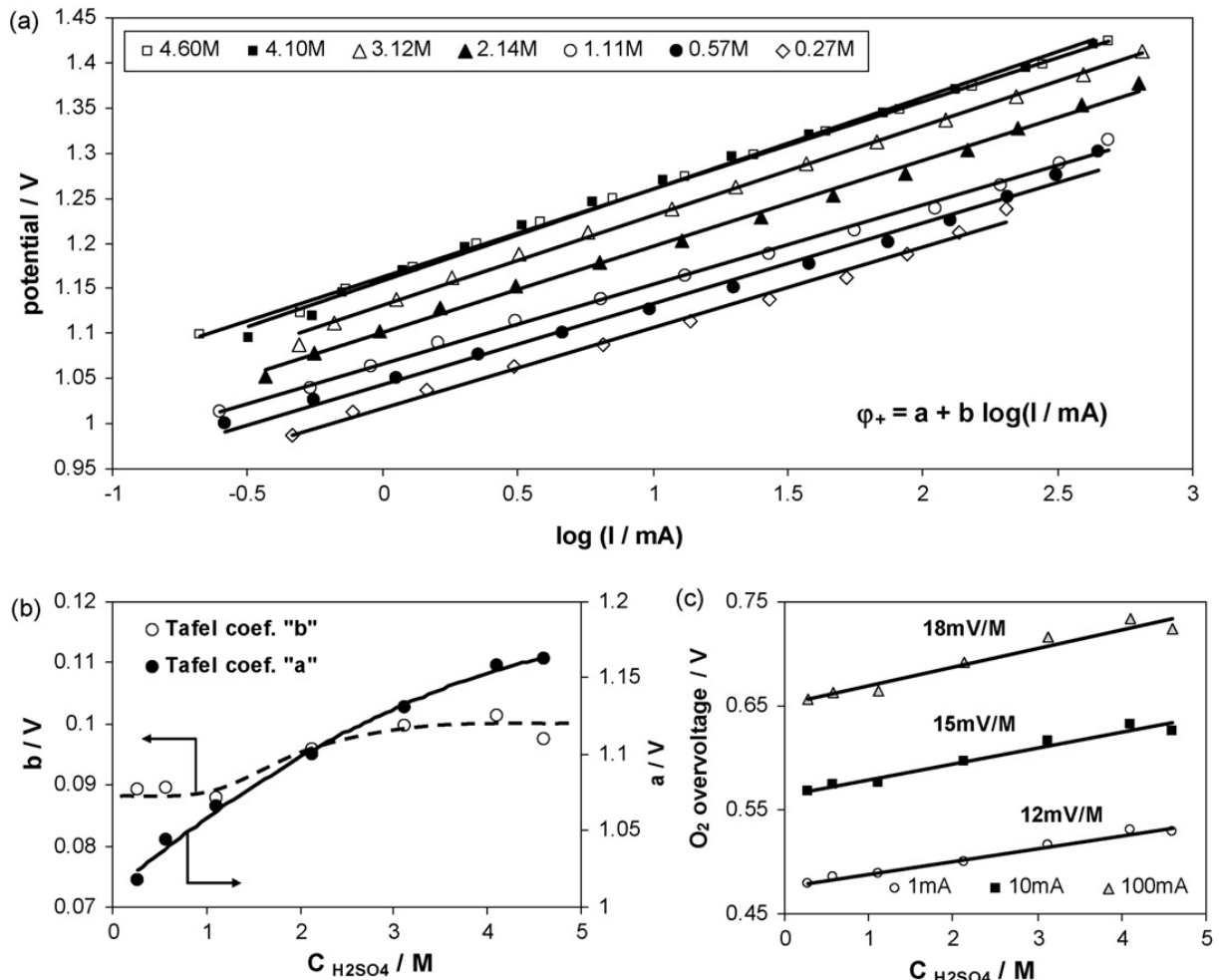
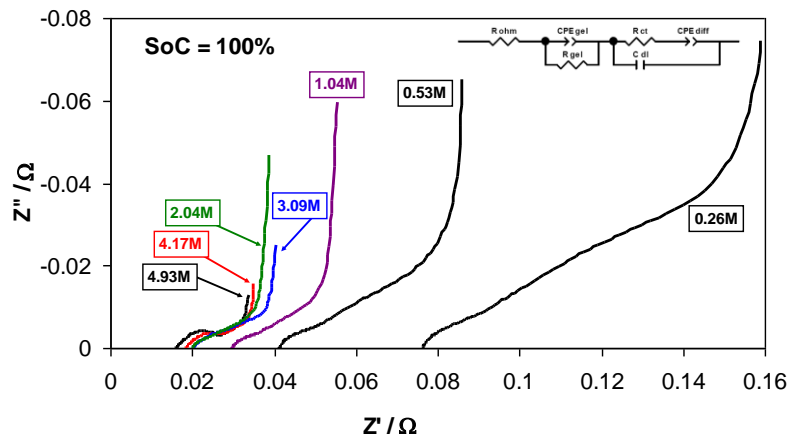


Fig. 3.6. (a) Tafel plots for the process of oxygen evolution in H₂SO₄ with different concentration. (b) Dependence of the Tafel coefficients on the H₂SO₄ concentration. (c) Dependence of the oxygen overvoltage on H₂SO₄ concentration [31].

In order to understand better the mechanism of influence of the electrolyte concentration on the positive plate performance different series of impedance spectroscopy measurements were performed at several different state of charge values in the electrolyte concentration range 0.25 – 5M H₂SO₄. Figure 3.7 presents a series of EIS in different electrolytes. Surprisingly, the Nyquist plots of the impedance does not change much from 4.93M to 2.04M H₂SO₄.

Fig. 3.7. Evolution of the positive plate impedance spectrum with the acid concentration at SOC = 100% during the “cycling” series in the frequency domain 50 kHz to 50 mHz [31].



However, the fitting of the spectra with the equivalent circuit discussed in paragraph 2.4.1 reveals some interesting trends presented in Figure 3.8. It can be seen that the ohmic resistance of the positive plates follows almost precisely the dependence of the specific resistance of the sulphuric acid on its concentration. Increasing the electrolyte concentration the charge transfer resistance decreases too in a similar fashion. These results confirm the suggestion that the minimum electrolyte concentration should be about 1.5-2M in order to avoid elevated ohmic drops at low SOC values. The dependence of the properties of the hydrated (gel) part of the lead dioxide on the sulphuric acid concentration was evaluated using the time constant time constant of the pair $R_{\text{gel}}CPE_{\text{gel}}$. The dilution of the electrolyte results in the increases of T_{gel} . This can be explained with the increase of the water content in the hydrated part of PbO_2 which decreases its electronic conductivity as well as decreased H^+ concentration which can decrease the ionic conductivity of this system [26]. The capacitance of the double layer increases with the electrolyte concentration quasi linearly. From one hand it can be related to increased surface charge density. From the other one can expect some adsorption effects. The second hypothesis was confirmed from the impedance spectra measured at different potentials in overcharge regime. The resulting C_{DL} vs. potential plots for different electrolytes are shown in Figure 3.9 featuring a minimum corresponding to the potential of zero charge (PZC). The shift of PZC towards higher potentials in more concentrated electrolytes indicates chemisorption of sulphate species [32]. The adsorption of the sulphuric species blocks the active sites for oxygen evolution and the gassing overvoltage increases explaining the family of Tafel plots presented in Figure 3.6a.

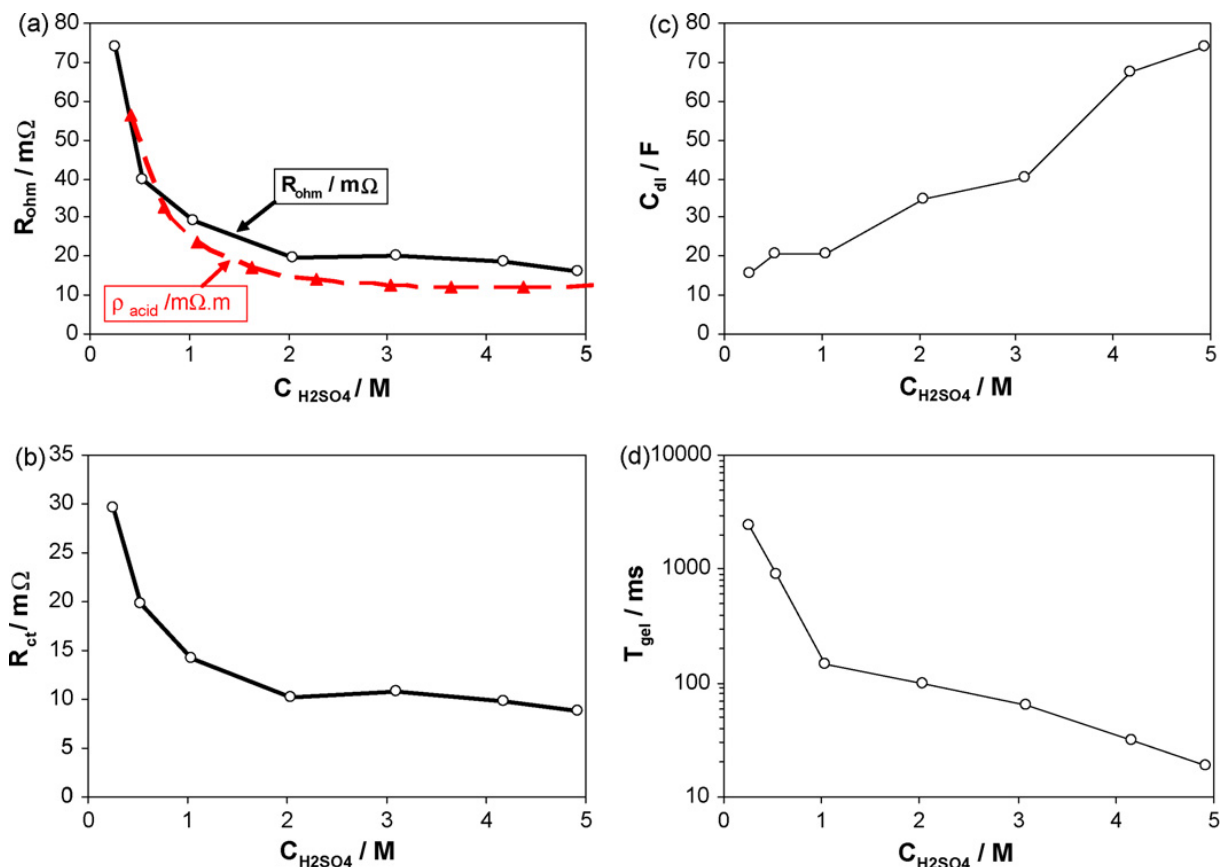


Fig. 3.8. Dependence of ohmic resistance (a), charge transfer resistance (b), EDL capacitance (c) and time constant of the gel part of the lead dioxide (d) on the H_2SO_4 concentration (3Ah positive plate at SOC = 100%) [31].

Fig. 3.9. Evolution of the EDL capacitance C_{dl} and oxygen evolution current with the potential in different H_2SO_4 electrolytes (working electrode 3Ah positive plate, Ag/Ag_2SO_4 reference electrode). The dashed line indicates the position on PZC [31].

3.1.3. Mechanism of the solid state passivation of the lead dioxide electrode

The passivation phenomenon in highly concentrated H_2SO_4 solutions ($C_{H_2SO_4} > 5M$) discussed in paragraph 3.1.1 was confirmed latter experimentally during battery cycling experiments carried out by Pavlov et al [30]. However, the question about the mechanism behind this phenomenon remained open. Some recent experiments carried out in CEA-LSE on lead dioxide / lead methanesulfonate electrodes threw new light on the passivation of the lead dioxide.

Yet different, there are a number of similarities between the $PbO_2/PbSO_4$ and $PbO_2/Pb(CH_3SO_3)_2$ electrode systems:

- Both the sulphuric acid and the methanesulfonic acid can be considered as non-oxidizing 1:1 electrolytes with similar pK_a and equivalent conductivity values [33]
- the structure of the methanesulfonate anion is similar to the bisulphate anion which is the predominant anion specimen in the sulphuric acid electrolyte
- the oxygen evolution on PbO_2 in methanesulfonic and sulphuric acid follows similar mechanism indicating chemisorption of methanesulfonate anions [34]

The main difference between both systems is in the high solubility of $Pb(II)$ methanesulfonate cations allowing the electrodeposition of thick and compact PbO_2 layers and their electro-dissolution without the formation of surface layer of insoluble compounds like the lead sulphate, i.e. dissolution without the precipitation of passivation layer. However, the cycling of PbO_2 electrode in MSA electrolytes revealed some quite unexpected results [35].

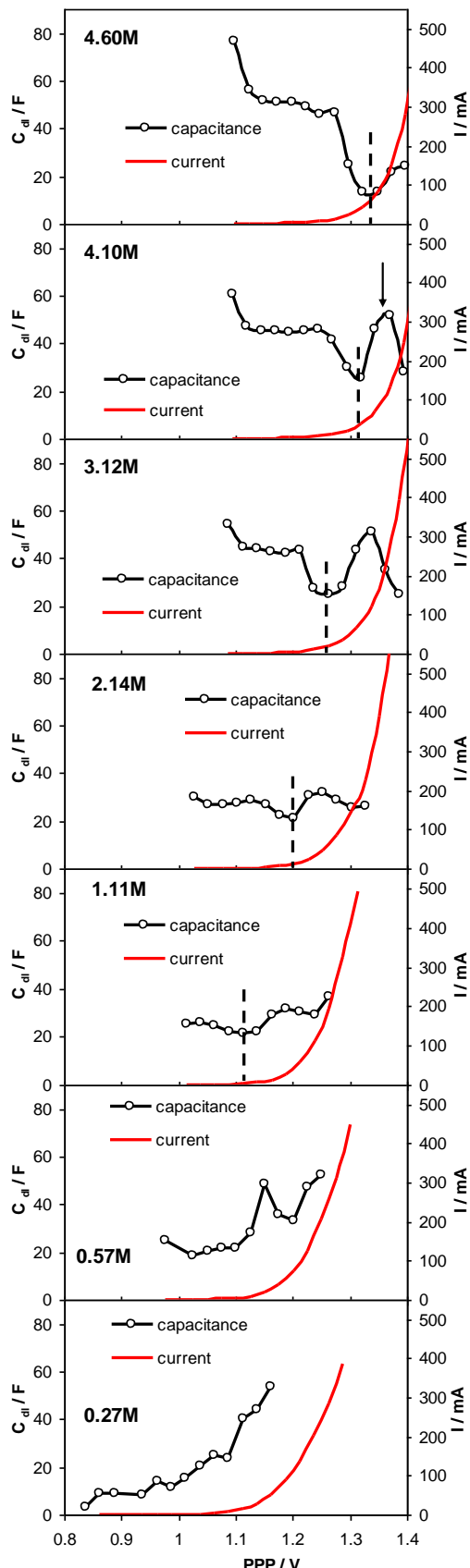


Figure 3.10 presents an example for such results. Here a dense compact layer of PbO_2 is electroplated on glass-like carbon disc electrode with $10mA/cm^2$ from a solution of $0.8M$ $Pb(II)$ + $1.6M$ MSA and further it is stripped with the same current density. The chrono-amperometric

calculation shows that 15% of the PbO_2 remains on the electrode in the end of the stripping. The impedance spectroscopy measurements performed in the denoted moments of the potential transient are also presented in Figure 3.10. They clearly indicate the presence of passivation layer with high ohmic resistance on the surface of the carbon electrode in the end of the striping stage. The subsequent recharge of the electrode begins with a sharp potential spike which is very similar to the one discussed by Pavlov et al. during the recharge of deeply discharged lead-acid battery positive plates with Sb-free grids [36]. Shortly after the spike, the impedance of the electrode returns to its “usual” levels indicating that the passivation layer is re-oxidized to highly conductive PbO_2 . What can explain the appearance of such passivation in a quasi-2D system without highly developed porosity and without the possibility for precipitation of insulating compounds?

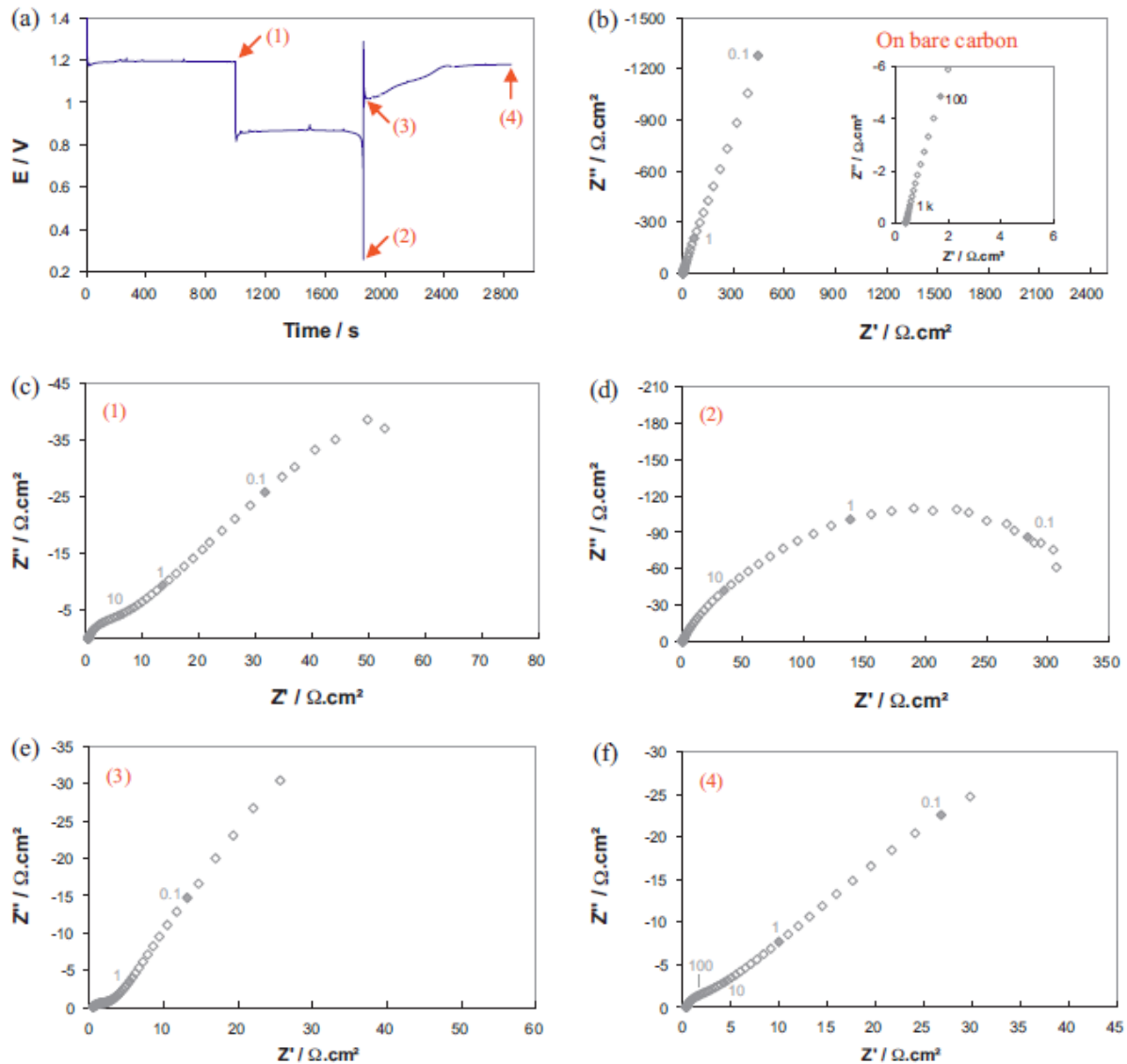


Fig. 3.10. Impedance spectra recorded during lead dioxide cycling in a $0.8\text{ M }Pb^{2+} + 1.6\text{ M }CH_3SO_3H$ electrolyte on vitreous carbon electrodes. (a) Potential response (vs. Ag/Ag_2SO_4); EIS spectra: (b) on bare carbon before the lead dioxide deposition, (c) after 1000 s of PbO_2 deposition, (d) after the electrodissolution, (e) at the early stage of the second deposition and (f) at the end of the second deposition. Current density: $\pm 10\text{ mA cm}^{-2}$. Cut-off potential for lead electrodissolution: 0.4 V. Values reported on EIS diagrams: frequency in Hz [35].

The explanation cannot be found in the thermodynamics of the system (Fig. 2.1). The application of X-diffraction also fails to identify some poorly conductive crystallographic phase [37].

The answer has been found using quartz crystal microbalance electrode (QCM) technique in the investigation of the kinetics of PbO_2 deposition and dissolution. Figure 3.11 presents the evolution of the mass of the electrode during deposition and dissolution of PbO_2 in 1M $\text{Pb}(\text{II}) + 0.2\text{M}$ MSA electrolyte with a current density of 10mA/cm^2 giving a zoom view in the end of the dissolution. It can be seen that the average mass gain is about 10% higher than the average mass loss. The latter supposes either a substantial oxygen evolution partial current or the accumulation of lead compound on the electrode surface, which dissolves rather slowly. The first hypothesis was rejected easily by side experiments of PbO_2 deposition on larger electrodes proving that the Faradic efficiency of the process is in the range of 99%. The zoom view of the end of the dissolution process (Fig. 3.11b) reveals even more interesting picture: the sharp drop of the electrode potential coincides with an abrupt change of the mass loss from $-979\mu\text{g/C}$ to $-260\mu\text{g/C}$. This result shows a very rapid accumulation of poorly soluble and highly ohmic compound.

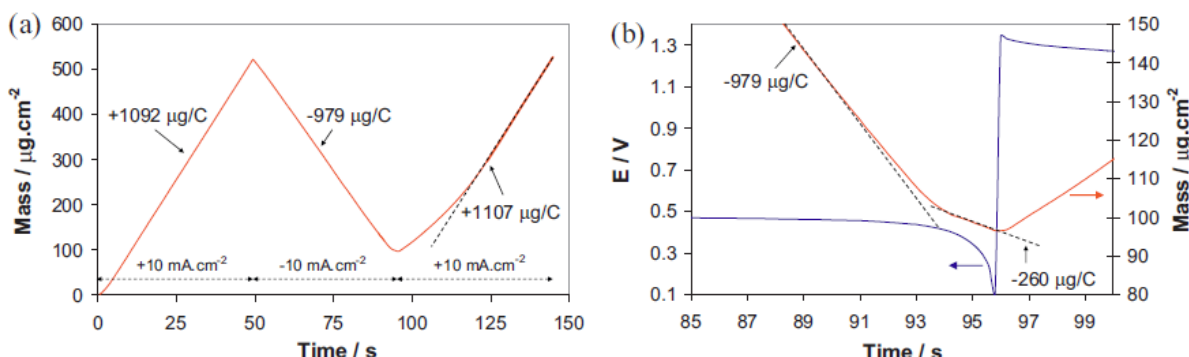
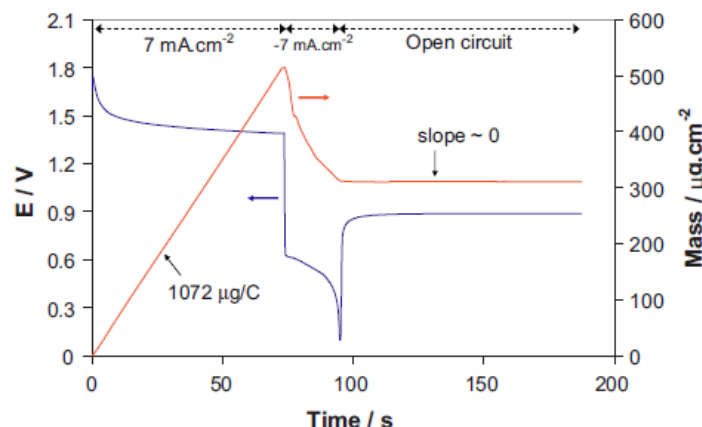


Fig. 3.11. Mass changes recorded at the beginning of PbO_2 cycling; (b) details of the mass changes together with the electrode potential (vs. $\text{Ag}/\text{Ag}_2\text{SO}_4$) at the end of the first reduction. Current density: $\pm 10 \text{ mA.cm}^{-2}$. Electrolyte: 1M $\text{Pb}^{2+} + 0.2\text{M} \text{CH}_3\text{SO}_3\text{H}$ [35].

The change of the electrolyte composition towards higher free acid concentration accelerates greatly the PbO_2 passivation process. Figure 3.12 demonstrates this statement for the case of 1M $\text{Pb}(\text{II}) + 1.5\text{M}$ MSA electrolyte. Here the passivation of the electrode occurs very early with an irregular mass loss evolution. After the drop of the potential the mass of the electrode does not change during the open circuit stay

Fig. 3.12. Mass changes and electrode potential evolution (vs. $\text{Ag}/\text{Ag}_2\text{SO}_4$) during the deposition and the partial reduction of PbO_2 , followed by an open circuit period, in 1M $\text{Pb}^{2+} + 1.5\text{M} \text{CH}_3\text{SO}_3\text{H}$. Current density: $\pm 7 \text{ mA cm}^{-2}$ [35].



The results from the experiments on QCM electrode show that the process of PbO_2 electro-dissolution proceeds by a solid-state mechanism with the active participation of H^+ cations. Figure 3.13 presents the mechanism of the PbO_2 stripping in solutions with low and high proton (free acid) concentration. According to the proposed mechanism the first step of the PbO_2 discharge is a solid state reduction with the participation of H^+ ions followed by chemical dissolution of the formed Pb(OH)_2 . The increase of the current density and the proton concentration shifts the reaction from the electrode surface towards the volume of the lead dioxide layer by H^+ insertion leading to the solid-state formation of hydrated non-stoichiometric lead oxides with both poor solubility in acid and high ohmic resistance.

The proposed mechanism explains very well the nature of the passivation process of $\text{PbO}_2/\text{PbSO}_4$ electrodes cycled in highly concentrated H_2SO_4 electrolytes despite the differences between this system and the $\text{PbO}_2/\text{Pb}(\text{CH}_3\text{SO}_3)_2$ electrode. It shows that at high acid concentrations the lead dioxide “prefers” to operate in a solid-state way, explaining the preferential formation of $\alpha\text{-PbO}_2$ and the corresponding loss of positive active material activity discussed in paragraph 3.1.1.

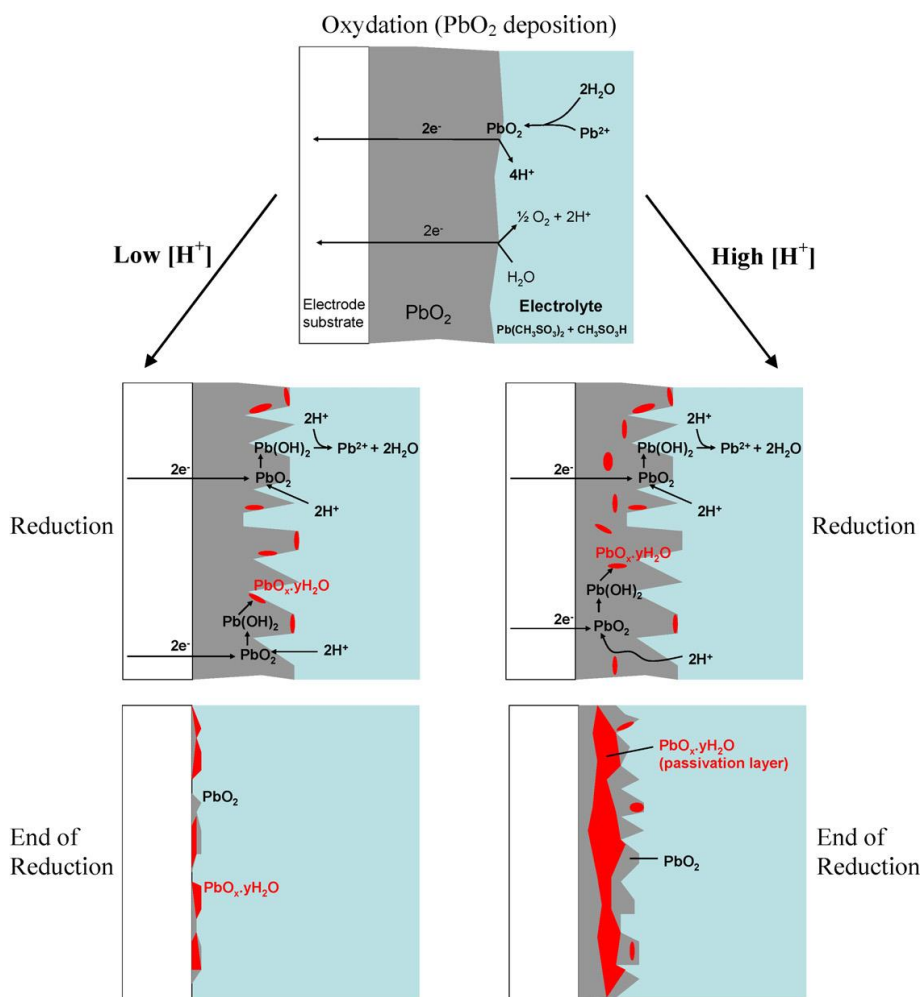


Fig. 3.13. Schematic representation of the possible mechanisms taking place during the electrodeposition and electrodissolution (at current densities $\geq 10 \text{ mA cm}^{-2}$) of a PbO_2 layer in a methanesulfonic acid solution containing: (left) a low amount of protons ($< 1 \text{ M}$) and (right) a high amount of protons ($> 1 \text{ M}$) [35].

3.2. Carbon honeycomb grids for advanced positive and negative plates

The grid is the basic element of the lead-acid battery. Its design and manufacturing technology did not change fundamentally since the invention of the pasting technology in the end of 19th century by another French chemist - Camille Alphonse Faure [38]. The pasted grids allowed obtaining much higher power and energy output from the lead-acid battery in comparison with the “Planté” electrodes. Despite the numerous advantages of the pasted and tubular grid technologies, the corresponding lead-acid batteries posses rather low energy density due to the insufficient utilisation of the lead metal, being in the range of 25-30% in total. The increase of this value is very important task in several different aspects:

- more efficient use of the lead can decrease the cost of the battery because its price is mainly formed by the price of the lead;
- the increase of the specific energy and power of the lead-acid battery without sacrificing its lifetime will make it more attractive for motive power and renewable energy storage applications;
- lead metal is a finite natural resource and it should be used in the most efficient way in the context of the ever increasing global energy and materials consumption.

The main drawback of the lead-acid battery grids is the high ratio between the quantity of the active material and the surface area of the current collector denoted by Pavlov as “ γ -coefficient” [39]. In attempt to find alternative lead-acid battery current collectors the carbon honeycomb grids were invented in CEA-INES [40]. Figure 3.14 presents the manufacturing scheme of the girds fabrication. The first step consists in the choice of composite honeycomb core material, which is suitable for carbonisation. It should satisfy two major requirements: the material should not change its shape at elevated temperatures and it should give a reasonable carbon yield after a pyrolysis up to 1000°C. Further, the honeycomb core is surrounded by a composite frame comprised by materials suitable for carbonisation. The resulting block is cut in slices with desired thickness, which are carbonized in inert atmosphere up to 1000°C. The obtained carbon/carbon composite combines a honeycomb structure, which can house the active material paste, with the distinctive shape of lead-acid battery plate having a lug for cast-on-strap connection and frame reinforcing greatly the otherwise delicate honeycomb structure.

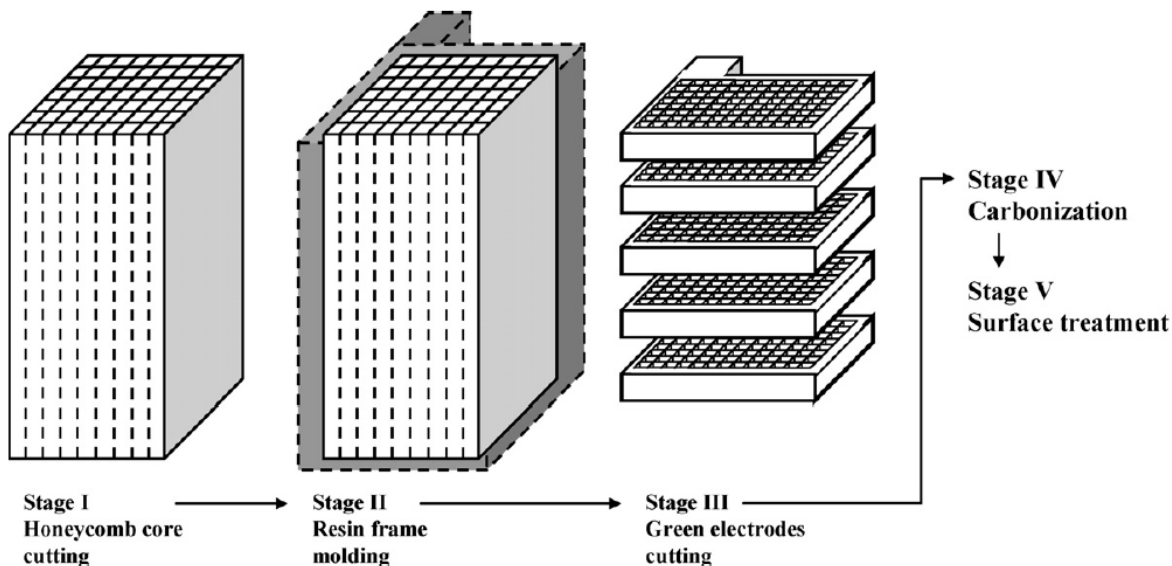


Fig. 3.14. Manufacturing scheme of the carbon honeycomb grid production [40].

The carbonised grid is enough conductive to allow the electrodeposition of different surface layers during the subsequent manufacturing steps. Figure 3.15 presents a photo of the first generation honeycomb grid prototypes. The starting materials were stacked corrugated paper scavenged from waste packaging, phenol-formaldehyde resin and cotton fibers for reinforcement of the frame. The resin was modified adding ethanol, which induces some porosity in the composite structure of the frame together with the cotton fibers. The latter allows very quick pyrolysis keeping perfectly the composite structure despite the severe linear shrinkage. Figure 3.15 illustrates this statement with grids carbonized from 200 to 1000°C in less than 5h [41].

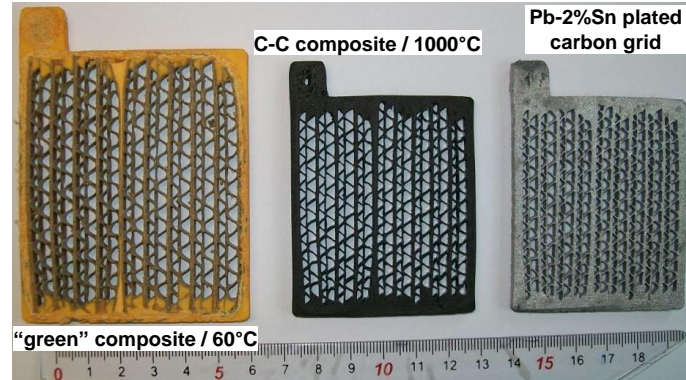


Fig. 3.15. Evolution of the carbon honeycomb grid after the sawing, the carbonisation and the lead–tin electroplating (the ruler below is in centimetres) [41].

Rough calculation of the grid geometric surface showed that the γ -coefficient of this grid is about 0.16–0.18 g_{AM}/cm². In the same time, the grid mesh size is much smaller than the one of the conventional grids, which supposes high energy and power outputs.

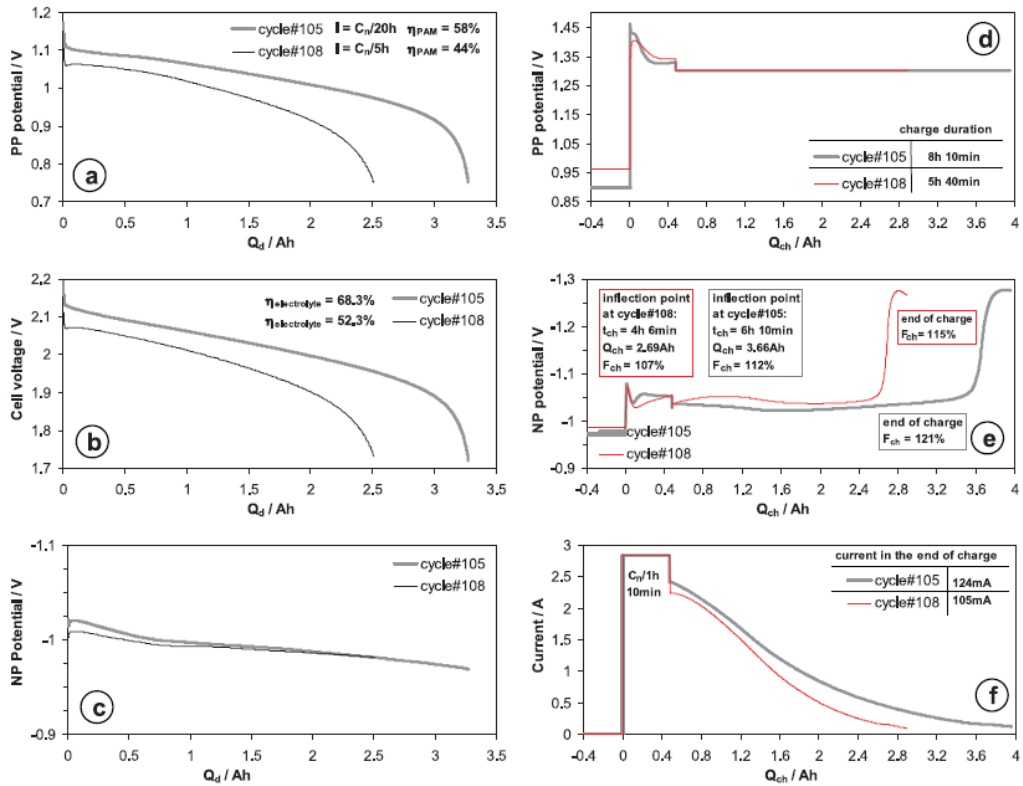


Fig. 3.16. Evolution of the VRLA cell parameters during cycle#105 and cycle#108 [41].

Figure 3.16 presents the performance of an AGM-VRLA cell comprised of honeycomb positive plate prototype encountered by a pair of traction negative plates and equipped with Ag/Ag₂SO₄

reference electrode after 104 cycles with Depth of Discharge (DOD) equal to 100%. The positive plate shows a fair active material utilisation in C/5h and C/20h discharge rate and rather good charge acceptance despite the plate thickness being about 4mm.

The post-mortem analysis of the positive plate after 190 cycles showed a softening of PAM probably due insufficient paste density as well as corrosion of both lead-tin coating and carbon/carbon composite. These results scheduled the main R&D perspectives: use of pastes with higher density and optimisation of the lead coating with improved control over the tin distribution, as well as addition of other alloying elements, which may improve the corrosion resistance of the grid. Another technological route is the increase of the honeycomb cell size (only for positive plate) allowing the use of thicker coatings. Such approach will decrease to certain degree the active material utilisation, but will improve greatly the battery lifetime.

All these problems are relevant only to the positive plate. The absence of grid corrosion phenomena at the negative plate offer much greater opportunities for the honeycomb technology there. Both the honeycomb cell size and the lead coating thickness can be minimized down to the levels corresponding to the optimal ohmic resistance and active mass utilization values.

Chapter 4

Conclusions

The successful charge management strategy for VRLA batteries is based on the suitable balance between charge and overcharge reactions. In order to find this balance, the electrochemistry of the oxygen cycle was studied in lead-acid cells with AGM separators equipped with reference electrodes and connected with gassing rate monitoring system. SEM observations and porosity data of both negative active material and AGM separator were used together with the DLVO theory of the thin liquid film stability to propose a theoretical approach for discussion of the oxygen recombination kinetics. According to this approach the negative plate is considered as a gas-diffusion electrode for oxygen reduction. Both the non-stationary and the stationary electrochemical kinetics of the oxygen recombination were studied varying different parameters like overcharge current, electrode potential, temperature and electrolyte saturation. The studies delivered some practical recommendations about the temperature, electrode potential and electrolyte saturation corresponding to an optimal compromise between the oxygen cycle current, efficiency and battery safety.

The electrochemical aspects of the pulse charge as an alternative battery management strategy were evaluated separately at the positive and the negative plate using electrochemical impedance spectroscopy. The latter provides data about the characteristic frequencies of the charge reactions. The application of a pulse charge with a frequency coinciding with the particular characteristic frequency leads to the appearance of electrochemical resonance in terms of maximal charge acceptance. The difference in the specific surface area and the structure of the double layer at the positive and the negative plate results in considerable difference between the characteristic frequencies at both electrodes. The latter means that the pulse charge can be used to solve issues related to the electrode with more problematic performance in the particular application.

The electrolyte appears as a critical component in the advanced lead-acid battery with a strong relation to the battery management strategy, energy and power density as well as the battery cost. It was demonstrated that electrolyte concentrations higher than 5mol/l could cause a passivation of the PbO₂ electrode accompanied by a capacity loss at the positive plate. QCM

electrodes of the PbO₂ electrodes in methanesulfonic acid solutions revealed that the phenomenon behind the passivation process is a solid-state PbO₂ reduction reaction with a proton insertion in the volume of the PbO₂ particles. The latter leads to the formation of hydrated non-stoichiometric lead oxides (PbO_n.xH₂O) with both poor electric conductivity and solubility in acidic solutions. The irreversibility of the process increases greatly with the decrease of the pH of the electrolyte.

The integration of Ag/Ag₂SO₄ reference electrode as an additional battery component offers a whole new scope of battery management solutions:

- control of the depth of discharge of the battery plate with more critical performance;
- charge algorithms controlling the oxygen evolution and the grid corrosion rate as well as avoiding the thermal runaway occurrence;
- individual electrode state of health and state of function diagnostics using impedance spectroscopy measurement;
- state of charge diagnostics based on the individual potential response of the positive or the negative plates.

Finally, the grids, which are the weakest battery component for a very long time, were optimised by the introduction of the carbon honeycomb grid concept. This new type of current collector is easy to manufacture and to optimise taking into account the particular battery application. They offer opportunities for energy and power density improvements as well as for battery cost reduction due to the higher percentage of global lead metal in use (in terms of grids and active materials).

Chapter 5

Research Perspectives

- Establishment of French group for R&D of redox-flow batteries

The French national electricity system is based on the nuclear power with a future perspective for stronger penetration of renewable energy generation. It is well known that the cost of both type of electricity production can be substantially reduced using large-scale energy storage. During the European project INVESTIRE Network: Investigations on Storage Technologies for Intermittent Renewable Energies: Evaluation and recommended R&D strategy, the cost performance analysis demonstrated that the redox-flow batteries are amongst the most promising large-scale energy storage system [42]. One can find numerous cross-points between the “classic” aqueous batteries (lead-acid, alkaline nickel) and the redox-flow batteries: water decomposition phenomena, corrosion, charge and discharge management, methods of characterisation etc. This experience can be used as a background for the establishment of a R&D redox-flow battery team as a part of the French National Institute for Solar Energy. Several actions have been already taken in this direction:

- During the project BEST “Benefits of storage systems for stationary grid-connected and advanced vehicle applications” (coordinated by Dr. Kirchev) an all-vanadium redox-flow system (10kW/100kWh CELLSTROM, Austria) was successfully integrated in the experimental electric grid of CEA-INES. The work was carried out by M. Nicolas MARTIN et M. Fabien CANAL, both tutored by Dr. Kirchev during their training period in the end of their engineering degree studies.

- Since October 2010, Dr. Kirchev is charged with the supervision of the PhD studies of M. Alexandre Oury. The topic of this thesis financed by ADEME is focused on the research and development of lead / methanesulfonic acid redox-flow battery. The first results were already an object of several peer-review publications and patent applications.
- In the end of the project BEST Dr. Kirchev started the research on low-cost zinc-based redox-flow systems. Several patent applications were filed.

The future redox-flow battery team will relay on the collaboration with the different CEA units as well as on the partnership with the academic structures in the Rhône-Alpes region LEPMI / INP Grenoble as well as the French Nation Petroleum Institute based in Lyon for the development of systems' components and models. Various French and European industrial groups were identified as future project partners in the development of different redox-flow battery component development: Arkema, BASF, DuPont, Société Bic, Mersen (former Carbone Loraine), SGL Carbon etc.

The redox-flow energy storage research and development can be divided in several axes which fit well in the overall strategy of the Laboratory for Storage of Electricity

➤ **Redox-flow battery management algorithms**

The management of the redox-flow battery storage differs markedly from the one of the classical battery systems. In addition to the typical current and voltage control, it requires the control of at least two pumping circuits as well as the real time estimation of both electrolytes composition in order to evaluate the system state (state of charge, state of health and state of function). All of this is of crucial importance in order to optimise the system performance in terms of efficiency and maintenance. The development of such algorithms requires two parallel research routes. In the first place, it is necessary to have simulation tools able to take into account both the reactors hydrodynamics and the battery electrochemistry. Having that information one can predict and schedule easily the required flow battery discharge power or charge acceptance. The second route includes the development of sensors for continuous monitoring of different electrolyte species using auxiliary electrolyte flow circuits. Such sensors can be electrochemical (potentiometric, amperometric, coulometric and impedimetric), optical (refractometric, colorimetric etc...) or mechanical (vibrating element transducer). Their purpose is to provide a real-time data to the BMS in order to evaluate state of charge, state of health (by the rate of cross-contamination between the positive and negative electrolyte), the water loss, and the available level of discharge power or charge acceptance capability.

➤ **Redox-flow battery couples and electrolytes**

The finding of suitable redox-flow battery electrolytes is still an open problem. The electrolytes should be inexpensive and stable over wide range of reagent concentrations and temperatures. It is also important to meet different safety requirements because large volumes of chemicals can be placed in close proximity to populated areas. They should be compatible with the ion-exchange membranes and the pumping circuits. Last, but not least, the electrochemical couples in the chosen electrolytes should be enough reversible. The recent progress in the vanadium redox-flow batteries shows that a combination of two or more anions can be particularly efficient strategy for increase of the reagents solubility [43]. Such approach offers a variety of combinations for both experimental and theoretical studies.

➤ **Reactors and components for redox-flow batteries**

The reactor is the core of the core unit of the energy conversion in the redox-flow battery. The reactor development is a typical multidisciplinary problem combining electrochemistry and corrosion science with the fluid dynamics and the chemical engineering. The first steps in this direction has been taken during the PhD thesis of M Alexandre Oury, where the carbon honeycomb technology has been used to develop innovative flow-trough electrodes for deposition and dissolution of lead dioxide from methanesulfonic acid electrolytes.

➤ **Polyaniline composite membranes**

The availability of low cost proton exchange membranes (PEM) with high cation selectivity is one of the most acute problems in the development of affordable redox-flow batteries. The usual strategy in the development of PEM materials includes co-polymerisation and further chemical functionalisation of various organics, which are subsequently melted or solution cast to form a thin membrane (Nafion® can be considered as the most typical for example). The redox-flow battery specifics allow the use of the polyaniline (PANI) as a promising alternative proton conducting material. The synthesis of this polymer (especially the electrochemical polymerisation) is very cheap and guarantees low final cost of the product. The use of PANI as proton exchange system is possible because the bi-polar flow reactor can be designed avoiding the physical contact between the membrane and the electrode (for example sandwiching the membrane between two glass mat tissue layers). In this way, the electric conductivity of PANI is eliminated and the latter operates only as proton exchange polymer. The nature of the partially or the fully oxidized protonated PANI is particularly suitable for composite membranes: this form of the polymer is insoluble in water, acid solutions and most of the typical organic solvents. Thus it can be mixed with suitable binders and extruded as non-porous sheets with various thickness. The study of the proton conductivity of the PANI apart from its electric conductivity is also very interesting from fundamental point of view, because almost all of the published literature discusses either its electric or mixed conductivity. The interest comes from the unique structure of this polymer where every monomer unit can be protonated, suggesting that the material can have extraordinary levels of proton conductivity. The first attempts for preparation of such membranes in the Laboratory for Storage of Electricity gave rather promising results despite the use of binders with strong deprotonating effect (base-catalyzed epoxy resin) [44].

- **Characterisation and modelling of different systems using electrochemical impedance spectroscopy**

The impedance-based battery modelling is a good compromise between the empiric and physical battery modelling. It allows the fast delivery of simulation tools in the context of the rapidly developing Li-battery market (multiple manufacturers / multiple electrochemistry technologies). The potential of this approach was demonstrated during the PhD thesis of Dr. Trung Kien Dong, which was co-supervised by Dr. Kirchev. Shortly after the publication of the thesis results of Dr. Trung Kien Dong in the Journal of the Electrochemical Society, the energy storage team of CEA-INES was contracted by a major Japanese industrial corporation for the development of impedance-based models for prediction and management of their proprietary Li-ion technology.

The impedance characterisation, especially those combined with Differential Impedance Analysis, is particularly interesting for the high power battery systems where one of the electrodes is partly (for example UltraBattery or carbon-doped lead-acid negative plates

recently denoted as lead-carbon or LC battery) or completely (Axion Pwer battery) replaced by a supercapacitive system (most often based on the activated carbon). In this way, the Faradic and the capacitive properties of large-scale cells and batteries can be divided and the high power behaviour of the system can be theoretically predicted. The impedance allows the in-situ monitoring of the ageing of such electrodes and it will point the further strategy for optimisation of such electrodes. The integration of different ageing mechanisms recognized partly or completely by the impedance spectroscopy and the Differential Impedance Analysis appears as a particularly challenging perspective in the development of the impedance based battery simulation tools.

The impedance spectroscopy is also particularly promising in the characterisation and the continuous control of some battery manufacturing processes, especially the formation process of both lead-acid and lithium-ion batteries. Such studies can be interesting for both the battery electrochemists and the industry engineers.

- Further optimisation of the lead acid battery technology

The lead-acid battery will remain the dominant technology on the market even in the next several decades [1]. Thus, the problems associated with the increase of the lead acid battery lifetime, specific energy and power will still be interesting for the industry and for the society. One step in this direction has been the development of the carbon honeycomb grid technology, which is particularly suitable for negative grids. Taking into account the nature of the corrosion process of the lead-acid battery positive grid and the narrow choice of suitable materials able to withstand such positive potentials and corrosive electrolyte media, it is clear that the titanium is amongst the best candidates for positive grid substrates. Here the main research perspective is the development of suitable surface treatment procedures for the creation of a long-lasting interface between the titanium and the lead dioxide active material.

References

1. Christophe Pillot, “The worldwide battery market 2011-2025”, Batteries 2012 - The 14th International Power supply Conference & exhibit 24th - 26th October 2012, Nice, France
2. S. Barnes and R. Mathieson, in D.H. Collins (ed.), Batteries 2, Pergamon Press, Oxford, 1965, pp. 41-52
3. D. Pavlov, “Lead-Acid Batteries: Science and Technology”, Chapter 14: Methods to restore the water decomposed during charge and overcharge of lead-acid batteries: VRLA Batteries, Elsevier B.V., Amsterdam, The Netherlands, 2011
4. R.F. Nelson in “Valve-Regulated Lead-Acid Batteries” (Eds. D.A.J. Rand, J. Garche, P.T. Moseley and C.D. Parker), Chapter 9 – Charging Techniques for VRLA Batteries, Elsevier B.V., Amsterdam, The Netherlands, 2004
5. D. Pavlov, V. Naidenov, S. Ruevski, V. Mircheva and M. Cherneva, “New modified AGM separator and its influence on the performance of VRLA batteries”, J. Power Sources, 113 (2003) 209
6. A. Kirchev, D. Pavlov and B. Monahov, “Gas-diffusion approach to the kinetics of oxygen recombination in lead-acid batteries”, J Power Sources, 113 (2003) 245
7. D. Pavlov, A. Kirchev and B. Monahov, “Mechanism of the oxygen cycle reactions proceeding at the negative plates of VRLA batteries”, J Power Sources”, 144 (2005) 521
8. A.J. Bard and L.R. Faulkner, “Electrochemical Methods: Fundamentals and Applications”, 2nd ed., John Wiley & Sons, Inc., New York, USA, 2001, p. 107.

9. A. Kirchev and D. Pavlov, "Influence of temperature and electrolyte saturation on rate and efficiency of oxygen cycle in VRLAB", J Power Sources, 162 (2006) 864
10. D. Pavlov, B. Monahov, A. Kirchev, D. Valkovska, "Thermal runaway in VRLAB-Phenomena, reaction mechanisms and monitoring", J Power Sources, 158 (2006) 689
11. P. Ruetschi, "Silver–silver sulfate reference electrodes for use in lead-acid batteries ", J Power Sources, 116 (2003) 53-60
12. P. Ruetschi, "Silver–silver sulfate reference electrodes for lead-acid batteries", J Power Sources 113 (2003) 363-370
13. A. Kirchev, "Reference electrode, manufacturing method and battery comprising the same", European Patent EP2106625 (A1), 2009-10-07
14. A. Kirchev, "Method of estimation of the state of charge of a lead-acid battery", International patent application WO 2009047581 (A1), 16 April 2009
15. D. Pavlov, T. Rogatchev, "Dependence of the phase composition of the anodic layer on oxygen evolution and anodic corrosion of lead electrode in lead dioxide potential region", Electrochim. Acta, 23 (1978) 1237
16. G.J. May, "Standby battery requirements for telecommunications power" J Power Sources 158 (2006) 1117
17. D. Benchetrite, "Optimisation de la recharge des accumulateurs au plomb à usage photovoltaïque", thèse Université de Picardie Jules Verne, 2004
18. F. Karoui, "Optimisation de stratégies de gestion des batteries au plomb utilisées dans les systèmes photovoltaïques", thèse INP Grenoble, 2007
19. Z. Stoynov and D. Vladikova, "Differential Impedance Analysis", Prof. Marin Drinov Academic Publishing House, Sofia, 2005
20. A. Kirchev, A. Delaille, M. Perrin, E. Lemaire, and F. Mattera, "Studies of the pulse charge of lead-acid batteries for PV applications. Part II. Impedance of the positive plate revisited", J Power Sources, 170 (2007) 495
21. P.T. Moseley, "Consequences of including carbon in the negative plates of Valve-regulated Lead-Acid batteries exposed to high-rate partial-state-of-charge operation", J Power Sources 191 (2009) 134
22. A. Kirchev, F. Mattera, E. Lemaire and T.K. Dong, "Studies of the pulse charge of Lead-acid batteries for PV applications Part IV: Pulse charge of the negative plate", J Power Sources 191 (2009) 82-90
23. C.H. Hsu and F. Mansfeld, "Concerning the conversion of the constant phase element parameter Y0 into a capacitance", Corrosion 57 (2001) 747-748
24. A.N. Frumkin, "The dependence of the double layer structure on the nature of the metal surface", J Res Catalysis Hokkaido Univ 15 (1967) 61
25. A. Kirchev, M. Perrin, E. Lemaire, F. Karoui and F. Mattera, "Studies of the pulse charge of lead-acid batteries for PV applications. Part I. Factors influencing the mechanism of the pulse charge of the positive plate", J Power Sources, 177 (2008) 217
26. Pavlov, "The Lead-Acid Battery Lead Dioxide Active Mass - a Gel-Crystal System with Proton and Electron Conductivity", J Electrochem Soc 139 (1992) 3075
27. H. Bode, "Lead – acid batteries", Wiley, New York, 1977, p. 27
28. B. Monahov, D. Pavlov, A. Kirchev and S. Vasilev, "Influence of pH of the H₂SO₄ solution on the phase composition of the PbO₂ active mass and of the PbO₂ anodic layer formed during cycling of lead electrodes", J Power Sources, 113 (2003) 281
29. D. Pavlov, A. Kirchev, M. Stoycheva and B. Monahov, "Influence of H₂SO₄ concentration on the mechanism of the processes and on the electrochemical activity of the Pb/PbO₂/PbSO₄ electrode", J Power Sources, 137 (2004) 288
30. D. Pavlov, V. Naidenov, S. Ruevski, "Influence of H₂SO₄ concentration on lead-acid performance: H-type and P-type batteries", J Power Sources 161 (2006) 658

31. **A. Kirchev**, A. Delaille, F. Karoui, M. Perrin, E. Lemaire, F. Mattera, "Studies of the pulse charge of lead-acid batteries for PV applications. Part III. Electrolyte concentration effects on the electrochemical performance of the positive plate", *J Power Sources*, 179 (2008) 808
32. B.N. Kabanov, I.G. Kiseleva, and D.I. Leykis, "Estimation of the potential of the zero charge on lead dioxide electrode", *Dokl. Acad. Nauk SSSR (Rus)*, 99 (1954) 805
33. M.D. Gernon, M. Wu, T. Buszta and P. Janney, "Environmental benefits of methanesulfonic acid: Comparative properties and advantages", *Green Chemistry* June 1999, p. 127
34. A. Oury, **A. Kirchev**, Y. Bultel, "Oxygen evolution on alpha-lead dioxide electrodes in methanesulfonic acid", *Electrochimica Acta* 63 (2012) 28-36
35. A. Oury, **A. Kirchev**, Yann Bultel, Eric Chainet, " $\text{PbO}_2/\text{Pb}^{2+}$ cycling in methanesulfonic acid and mechanisms associated for soluble lead acid flow battery applications", *Electrochimica Acta*, 71 (2012) 140-149
36. D. Pavlov, G. Petkova, "Phenomena that limit the capacity of the positive lead acid battery plates. 1. The charge potential transient as an indicator of positive plate state of charge and state of health", *J. Electrochem. Soc.*, 149 (2002) A644
37. X. Li, D. Pletcher, F.C. Walsh, "A novel flow battery: A lead acid battery based on an electrolyte with soluble lead(II). Part VII. Further studies of the lead dioxide positive electrode", *Electrochimica Acta* 54 (2009) 4688–4695
38. E.Y. Weissman in "Batteries. Vol. 2: Lead-acid batteries and Electric Vehicles" (ed. K.V. Kordesch), Chapter 1 "Lead-acid storage batteries", Dekker, New York, 1977, p. 4
39. D. Pavlov, *J Power Sources* 53 (1995) 9
40. **A. Kirchev**, N. Kircheva, Electrode de batteries acide-plomb comportant un reseau de pores traversants et procédé de fabrication, French patent application FR 2944151 (A1), 2010-10-08
41. **A. Kirchev**, N. Kircheva, M. Perrin, "Carbon honeycomb grids for advanced lead-acid batteries. Part I: Proof of concept", *J Power Sources*, 196 (2011) 8773
42. Investire Network Project website site web: www.itpower.co.uk/investire/index.html
43. L. Li, S. Kim, W. Wang, M. Vijayakumar, Z. Nie, B. Chen, J. Zhang, G. Xia, J. Hu, G. Graff, J. Liu, Z. Yang, *Advanced Energy Materials*, 1 (2011) 394-400.
44. **A. Kirchev**, B. Diem, F. Mattera, ELECTRODE DE REFERENCE MINIATURE, French patent application FR2962806 (A1) - 2012-01-20

Curriculum Vitae

Angel KIRCHEV

Ingénieur de recherche / Chef de projet au Laboratoire du Stockage de l'Electricité, Institut National de l'Energie Solaire (CEA-INES)

Expert du CEA dans le domaine Chimie & génie chimique avec la spécialité électrochimie

Formation

- 2001 - 2005 Doctorat en Electrochimie et Stockage de l'Energie
Académie Bulgare des Sciences – Institut de l'Electrochimie et des Systèmes d'Energie (BAS-IEES)
- 1995 – 2000 Master en Chimie (BAC+5) avec spécialisation Physico-chimie et Chimie Théorique, major de promotion
- 1984 – 1995 Baccalauréat, option Biologie et Chimie

Domaines d'Etudes

- Stockage de l'énergie électrochimique
Electrochimie et corrosion
Spectroscopie d'impédance électrochimique
Modélisation des accumulateurs électrochimiques
Systèmes de gestion des batteries (Battery Management Systems)
Composites Carbone / Carbone

Expériences Professionnelles

- Depuis Juillet 2007** **Ingénieur de recherche / Chef de projet** au Laboratoire du Stockage de l'Electricité, Institut National de l'Energie Solaire (CEA-INES)
Mission : Développement de BMS pour batteries plomb-acide, Li-ion, Ni-MH et Ni-Cd ; Développement de batteries au plomb avancées et de batteries redox-flow ; Développement de capteurs pour BMS ; Modélisation des batteries en spectroscopie d'impédance ; Développement de composites Carbone/Carbone pour électrodes tridimensionnelles
- 2005 – 2007** **Post-doc** (24 mois) au Laboratoire du Stockage de l'Electricité, Institut National de l'Energie Solaire (CEA-INES)
Mission : Développement d'algorithmes de charge pulsée pour accumulateurs au plomb pour des applications solaires ; Développement de BMS et d'outils de diagnostiques de l'Etat de Charge et de l'Etat de Santé des accumulateurs aqueux (plomb-acide et alcalins)
- 2004 – 2005** **Chercheur [ou ingénieur de recherche]** au laboratoire des accumulateurs au plomb de l'Institut de l'Electrochimie et des Systèmes d'Energie - Académie Bulgare des Sciences – (BAS-IEES)

Mission : implication dans les projets de recherche et de développement des accumulateurs au plomb

2001 - 2003 **Doctorant** au laboratoire des accumulateurs au plomb de l’Institut de l’Electrochimie et des Systèmes d’Energie - Académie Bulgare des Sciences – (BAS-IEES)

Sujet de thèse : « Gas Diffusion Kinetics of Oxygen Reduction on the Negative Plate of VRLAB »

Autres Missions : implication dans des projets divers sur l’électrochimie du plomb et la technologie des accumulateurs au plomb étanchés [je dirais étanches] – AGM

Mars 2000 – Décembre 2000 **Technicien de recherche** au laboratoire des accumulateurs au plomb de l’Institut de l’Electrochimie et des Systèmes d’Energie - Académie Bulgare des Sciences – (BAS-IEES)

Mission : étude de l’évolution de l’oxygène et de la corrosion anodique des alliages plomb-étain

Prix et distinctions

« Dave Rice Research Award » attribué aux jeunes chercheurs pour leurs contributions aux domaines de la science et de la technologie des accumulateurs au plomb, Avril 2005

Gestion des recherches

Participation à la rédaction de diverses demandes de financement et de bilans de recherche :

- Advanced Lead-Acid Battery Consortium
- European Research Office of the U.S. Army
- EC Framework 5 et 7
- Agence Nationale de la Recherche
- E.ON International Research Initiative
- Direction générale de l’armement
- Projets industriels bilatéraux (SAFT, One-Too, NEC, Serma Technologies)

Coordination des projets :

2008 – 2011 Projet BEST « Benefits of storage systems for stationary grid-connected and advanced vehicle applications », collaboration entre l’équipe du Laboratoire du Stockage de l’Électricité (CEA-INES) et celle du Electrochemical Energy Conversion and Storage Systems Group (EEC Storage Systems), RWTH Aachen University, financée par - E.ON International Research Initiative

2011 - 2013 Projet CARBOLEAD 2010 « Nouvelles grilles de carbone pour accumulateurs légers à électrodes de plomb », collaboration entre l’équipe du Laboratoire du Stockage de l’Électricité (CEA-INES), l’équipe Surface et Interface : réactivité chimique des matériaux de l’Institut Jean Lamour (Université de Nancy), Material Mates (M²) et STECO Power financée par l’Agence Nationale de la Recherche

Co-encadrement d'étudiants

- 2011 – 2013** **Alexandre Oury**, Thèse sur le développement des batteries redox-flow plomb / acide méthanesulfonique
Thèse dirigée par le professeur Yann Bultel (LEPMI / INP Grenoble), co-encadrement par A. Kirchev
- 2007 – 2010** **Trung Kien Dong**, Thèse sur la modélisation des batteries li-ion basée sur la Spectroscopie d'Impédance Electrochimique (date de soutenance le 19 juillet 2010)
Thèse dirigé par le professeur Yann Bultel (LEPMI / INP Grenoble), co-encadrement par Florence Mattera (25%) et A. Kirchev (75%)
- 2010** **Jessy Rolling**, Stage de 5 mois sur la caractérisation des batteries ZEBRA par Spectroscopie d'Impédance Electrochimique
- 2010** **Romain Grandveau**, Stage de 4 mois sur le développement des grilles nid d'abeilles en composite carbone/carbone
- 2010** **Fabien Canal**, Stage de 6 mois sur le développement des batteries redox en circulation
- 2009** **Nicolas Martin**, Stage de 6 mois sur la modélisation des batteries Ni-MH basée sur la Spectroscopie d'Impédance Electrochimique

Activités d'enseignement

Formation d'un groupe d'ingénieurs de la société Inci Akü (fabricant d'accumulateurs au plomb basé en Turquie) sur le thème « Construction, exploitation et impédance des accumulateurs au plomb » (12 heures)

Formation d'un groupe d'ingénieurs de la société NEC (Japon) sur le thème « Spectroscopie d'impédance des accumulateurs électrochimiques » (4 heures)

Activités d'expertise

Selecteur d'articles scientifiques de Journal of Power Sources et Journal of the Electrochemical Society

Co-organisation de congrès

5th International conference on Lead-Acid Batteries LABAT'02, 10-13 June 2002, Varna, Bulgaria

6th International conference on Lead-Acid Batteries LABAT'2005, 13-16 June 2005, Varna, Bulgaria

Collaborations

RWTH – ISEA (Aix le Chapelle), LEPMI – INP Grenoble, Institut Jean Lamour - CP2S, Académie Bulgare des Sciences - IEES

Production scientifique

18 publications à des revues électrochimiques, 15 publications à des actes de conférences, 11 dépôts de brevets, 17 présentations à des conférences, 6 communications par posters

List of publications in periodic journals

1. B. Monahov, D. Pavlov, A. Kirchev and S. Vasilev, "Influence of pH of the H₂SO₄ solution on the phase composition of the PbO₂ active mass and of the PbO₂ anodic layer formed during cycling of lead electrodes", J Power Sources, 113 (2003) 281
2. A. Kirchev, D. Pavlov and B. Monahov, "Gas-diffusion approach to the kinetics of oxygen recombination in lead-acid batteries", J Power Sources, 113 (2003) 245
3. D. Pavlov, A. Kirchev, M. Stoycheva and B. Monahov, "Influence of H₂SO₄ concentration on the mechanism of the processes and on the electrochemical activity of the Pb/PbO₂/PbSO₄ electrode", J Power Sources, 137 (2004) 288
4. D. Pavlov, A. Kirchev and B. Monahov, "Mechanism of the oxygen cycle reactions proceeding at the negative plates of VRLA batteries", J Power Sources", 144 (2005) 521
5. D. Pavlov, B. Monahov, A. Kirchev, D. Valkovska, "Thermal runaway in VRLAB-Phenomena, reaction mechanisms and monitoring", J Power Sources, 158 (2006) 689
6. A. Kirchev and D. Pavlov, "Influence of temperature and electrolyte saturation on rate and efficiency of oxygen cycle in VRLAB", J Power Sources, 162 (2006) 864
7. A. Kirchev, M. Perrin, E. Lemaire, F. Karoui and F. Mattera, "Studies of the pulse charge of lead-acid batteries for PV applications. Part I. Factors influencing the mechanism of the pulse charge of the positive plate", J Power Sources, 177 (2008) 217
8. A. Kirchev, A. Delaille, M. Perrin, E. Lemaire, and F. Mattera, "Studies of the pulse charge of lead-acid batteries for PV applications. Part II. Impedance of the positive plate revisited", J Power Sources, 170 (2007) 495
9. A. Kirchev, A. Delaille, F. Karoui, M. Perrin, E. Lemaire, F. Mattera, "Studies of the pulse charge of lead-acid batteries for PV applications. Part III. Electrolyte concentration effects on the electrochemical performance of the positive plate", J Power Sources, 179 (2008) 808
10. A. Kirchev, F. Mattera, E. Lemaire and T.K. Dong, "Studies of the pulse charge of Lead-acid batteries for PV applications Part IV: Pulse charge of the negative plate", J Power Sources 191 (2009) 82-90
11. T. K. Dong, A. Kirchev, F. Mattera, and Y. Bultel, "Modeling of Lithium Iron Phosphate Batteries by an Equivalent-electrical Circuit: Method of Model Parameterization and Simulation", ECS Transactions 25 (issue 35) 131-138, 2010
12. T.K. Dong, A. Kirchev, F. Mattera, J. Kowal, Y. Bultel, "Dynamic modeling of Li-ion batteries using an equivalent electrical circuit", J Electrochem Soc 158 (2011) A326-A336
13. A. Kirchev, N. Kircheva, M. Perrin, "Carbon honeycomb grids for advanced lead-acid batteries. Part I: Proof of concept", J Power Sourcees, 196 (2011) 8773
14. T. K. Dong, M. Montaru, A. Kirchev, M. Perrin, F. Lambert and Y. Bultel, Modeling of Lithium Iron Phosphate Batteries by Equivalent Electrical Circuit: Part II – Model Parameterization as Function of Power and State of Energy (SOE), ECS Transactions, vol. 35, issue 32, (2011) 229-237
15. A. Oury, A. Kirchev, Yann Bultel, "Oxygen evolution on alpha-lead dioxide electrodes in methanesulfonic acid", Electrochimica Acta 63 (2012) 28-36
16. A. Oury, A. Kirchev, Y. Bultel, E. Chainet, "PbO₂/Pb²⁺ cycling in methanesulfonic acid and mechanisms associated for soluble lead acid flow battery applications", Electrochimica Acta, 71 (2012) 140-149

17. A. Oury, A. Kirchev, Y. Bultel, "New elements about lead dioxide/lead(II) cycling in methanesulfonic acid", ECS Transactions, in press
18. A. Oury, A. Kirchev, and Y. Bultel, "Potential Response of Lead Dioxide/Lead(II) Galvanostatic Cycling in Methanesulfonic Acid: A Morphologico-Kinetics Interpretation", J. Electrochem. Soc. 160 (2013) A148

List of publications in conference proceedings

1. B. Monahov, A. Kirchev, S. Vasilev and D. Pavlov, "Influence of pH on the structure and phase composition of PbO₂ anodic layers formed on Pb electrodes in H₂SO₄ solutions", Proceedings of the International conference LABAT-02, p.51, Sofia, June 2002.
2. A. Kirchev, D. Pavlov and B. Monahov, "Gas diffusion approach to the kinetics of oxygen recombination in lead acid batteries", Proceedings of the LABAT-02 International conference, p.131, Sofia, June 2002
3. B. Monahov, D. Pavlov, G. Papazov, A. Kirchev, M. Stoycheva, S. Vassilev and M. Cherneva, "Influence of the phenomena occurring during PSoCduy on the performance of VRLA batteries", Proceedings of the STORE conference - "Storage for Renewable Energies", Aix-en-Provence, October 2003
5. A. Kirchev, D. Pavlov, B. Monahov and A. Gigova, "Temperature dependence of the oxygen recombination reaction in valve regulated lead acid batteries", Proceedings of the STORE conference - "Storage for Renewable Energies", Aix-en-Provence, October 2003
6. A. Kirchev, D. Pavlov and B. Monahov, "A method for investigation of the stationary electrochemical kinetics of O₂ recombination in valve regulated lead acid (VRLA) batteries", Proceedings of the International Workshop "Advanced Techniques for Energy Sources Investigation and Testing", 4th - 9th September 2004, Sofia, Bulgaria
7. A. Kirchev, D. Pavlov and A. Gigova, "Effect of electrolyte saturation on rate and efficiency of oxygen cycle in VRLAB", Proceedings of the International conference LABAT-05, p. 25, Sofia, June 2005
8. D. Pavlov, B. Monahov, A. Kirchev, D.S. Valkovska, "Thermal Phenomena in VRLAB", Proceedings of the International conference LABAT-05, p. 5, Sofia, June 2005
9. D.S. Valkovska, D. Pavlov, A. Kirchev, "Heat Generation in VRLA Battery – Influence of Separator Type", Proceedings of the International conference LABAT-05, p. 19, Sofia, June 2005
10. A. Kirchev, M. Perrin, E. Lemaire, F. Karoui and F. Mattera, "Factors influencing the mechanism of the pulse charge of the lead-acid battery positive plate", Proceedings of the 10th European Lead Battery Conference, Athens, Greece, 26–29 September 2006
11. A. Kirchev, F. Mattera, J. Merten, "Impedance characterization of silicon PV cells and modules", Proceedings of the 22nd European Photovoltaic Solar Energy Conference, 3-7 September 2007, Milan, Italy, p. 360
12. A. Kirchev, F. Mattera, E. Lemaire, K. Dong, "Pulse charge of the lead-acid battery plate – influence of the state of charge and frequency on the reaction mechanism", Proceedings of the 7th International Conference on Lead-Acid Batteries LABAT 2008, 9-12 June, Varna, Bulgaria, p. 161
13. T.K. Dong, A. Kirchev, F. Mattera, A. Delaille, "Integration of lithium-ion battery in photovoltaic applications: Impedance characterization and electric equivalent circuit

modelling”, Proceedings of the Advanced Automotive Battery Conference, 14-16 May 2008, Tampa, Florida, USA

14. A. Kirchev, N. Kircheva, M. Perrin, “Carbon honeycomb grids for advanced VRLAB negative plates”, Proceedings of the 8th International Conference on Lead-Acid Batteries LABAT’2011, 7-10 June, Albena, Bulgaria, p. 19

15. Dirk Magnor, Angel Kirchev, Dirk Uwe Sauer, “Economic Assessment and Design Optimization of PV-Battery Systems in Rural and Off-grid Electrification Applications”, proceedings of the 2nd Symposium Small PV-Applications, 6-7 June 2011, Ulm, Germany

Patent applications

1. A. Kirchev, REFERENCE ELECTRODE, MANUFACTURING METHOD AND BATTERY COMPRISING SAME, European Patent EP2106625 (A1), 2009-10-07
2. A. Kirchev, METHOD OF ESTIMATION OF THE STATE OF CHARGE OF A LEAD-ACID BATTERY, International patent application WO 2009047581 (A1), 16 April 2009.
3. A. Kirchev, PROCÉDÉ D'ESTIMATION DE L'ÉTAT DE CHARGE D'UNE BATTERIE, International patent application WO2009136222 (A1), 2009-11-12
4. A. Kirchev, ELECTRODE FOR LEAD-ACID BATTERY AND METHOD FOR PRODUCING SUCH AN ELECTRODE, International patent application WO2009150485 (A1), 2009-12-17
5. A. Kirchev, N. Kircheva, CELLULE ELECTROCHIMIQUE A FLUX D'ELECTROLYTE COMPORTANT DES ELECTRODES TRAVERSANTES ET PROCEDE DE FABRICATION, French patent application FR 2944031 (A1), 2010-10-08
6. A. Kirchev, N. Kircheva, ELECTRODE DE BATTERIE ACIDE-PLOMB COMPORTANT UN RESEAU DE PORES TRAVERSANTS ET PROCEDE DE FABRICATION, French patent application FR 2944151 (A1), 2010-10-08
7. T.K. Dong, A. Kirchev, F. Mattera, METHOD FOR CHARACTERISING AN ELECTRIC BATTERY, French patent application FR 2948771 (A1), 2011-02-04
8. A. Kirchev, BATTERIE METAL-AIR A FLUX D'ELECTROLYTE, French patent application FR 2952476 (A1), 2011-05-13
9. A. Kirchev, PROCEDE DE DIAGNOSTIC DE L'ETAT DE SANTE D'UNE BATTERIE, N° de brevet : FR2955670 (A1), 2011-07-29
10. A. Kirchev, B. Diem, F. Mattera, ELECTRODE DE REFERENCE MINIATURE, French patent application FR2962806 (A1) — 2012-01-20
11. A. Kirchev, HIGH CAPACITY GASEOUS DIFFUSION ELECTRODE, WO2013007887 (A1) - 2013-01-17

Conference presentations

1. B. Monahov, A. Kirchev, S. Vasilev and D. Pavlov, “Influence of pH on the structure and phase composition of PbO₂ anodic layers formed on Pb electrodes in H₂SO₄ solutions”, lecture held by B. Monahov during the International conference LABAT-02, Varna, Bulgaria, 10-13 June, 2002

2. A. Kirchev, D. Pavlov and B. Monahov, "Gas diffusion approach to the kinetics of oxygen recombination in lead acid batteries", lecture held by A. Kirchev during the LABAT-02 International conference, Varna, Bulgaria, 10-13 June, 2002
3. B. Monahov, D. Pavlov, G. Papazov, A. Kirchev, M. Stoycheva, S. Vassilev and M. Cherneva, "Influence of the phenomena occurring during PSoC duty on the performance of VRLA batteries", lecture held by B. Monahov during the STORE conference - "Storage for Renewable Energies", Aix-en-Provence, France, 20-21 October 2003
4. A. Kirchev, D. Pavlov, B. Monahov and A. Gigova, "Temperature dependence of the oxygen recombination reaction in valve regulated lead acid batteries", lecture held by A. Kirchev during the STORE conference - "Storage for Renewable Energies", Aix-en-Provence, France, 20-21 October 2003
5. A. Kirchev, D. Pavlov, "Influence of temperature and electrolyte saturation on rate and efficiency of oxygen cycle in VRLAB", invited lecture held by A. Kirchev during the 24th International Power Sources Symposium, Brighton, UK, 18-21 April, 2005
6. A. Kirchev, D. Pavlov and A. Gigova, "Effect of electrolyte saturation on rate and efficiency of oxygen cycle in VRLAB", lecture held by A. Kirchev during the International conference LABAT-05, Varna, Bulgaria, 13-16 June 2005
7. D. Pavlov, B. Monahov, A. Kirchev, D.S. Valkovska, "Thermal Phenomena in VRLAB", lecture held by D. Pavlov during the International conference LABAT-05, Varna, Bulgaria, 13-16 June 2005
8. A. Kirchev, M. Perrin, E. Lemaire, F. Karoui and F. Mattera, "Factors influencing the mechanism of the pulse charge of the lead-acid battery positive plate", lecture held by M. Perrin during the 10th European Lead Battery Conference, Athens, Greece, 26–29 September 2006
9. A. Kirchev, F. Mattera, E. Lemaire, K. Dong, "Pulse charge of the lead-acid battery plate – influence of the state of charge and frequency on the reaction mechanism", lecture held by A. Kirchev during the 7th International Conference on Lead-Acid Batteries LABAT 2008, 9-12 June, Varna, Bulgaria, p. 161
10. A. Kirchev, N. Kircheva, M. Perrin, R. Grandveau, "Carbon honeycomb grids for high energy density lead acid batteries", lecture held by A. Kirchev during the 12th European Lead Battery Conference (ELBC), September 21-24, 2010, Istanbul, Turkey
11. T.K. Dong, A. Kirchev, F. Mattera, and Y. Bultel, "Modeling of Lithium Iron Phosphate Batteries by an Equivalent Electrical Circuit: Method of Model Parameterization and Simulation", lecture held by T.K. Dong during the 216th ECS Meeting, October 4 - October 9, 2009, Vienna, Austria
12. T.K. Dong, A. Kirchev, M. Perrin, F. Mattera and Y. Bultel, "Modeling of Lithium Iron Phosphate Batteries by Equivalent Electrical Circuit: Part II - Model Parameterization as Function of Power and State of Energy (SOE)", lecture held by Y. Bultel during the 219th ECS Meeting, Montreal, Canada, 1-6 May 2011
13. A. Kirchev, "Evaluation of Carbon Honeycomb Grids for Positive and Negative Lead-Acid Battery Plates", invited lecture during the 123rd Convention of Battery Council International, Miami, USA, 1-4 May 2011
13. A. Kirchev, N. Kircheva, M. Perrin, "Carbon honeycomb grids for advanced VRLAB negative plates", lecture held by A. Kirchev during the 8th International Conference on Lead-Acid Batteries LABAT'2011, 7-10 June, Albena, Bulgaria

14. D. Magnor, A. Kirchev, D.U. Sauer, "Economic Assessment and Design Optimization of PV-Battery Systems in Rural and Off-grid Electrification Applications", lecture held by D. Magnor during the 2nd Symposium Small PV-Applications, 6-7 June 2011, Ulm, Germany
15. R. Christin, N. Martin, A. Kirchev, D.U. Sauer, J. Kowal, "Ranking the merits of battery technologies: Impedance studies of ZEBRA cells during the project BEST", lecture held by A. Kirchev during the E.ON International Research Initiative Conference, Birmingham, UK, 5-6 July 2011
16. D. Magnor, A. Kirchev, D.U. Sauer, "Economic Assessment and Design Optimization of PV-Battery Systems in Rural and Off-grid Electrification Applications", lecture held by D. Magnor during the 2nd Symposium Small PV-Applications, 6-7 June 2011, Ulm, Germany
17. Oury, A. Kirchev and Y. Bultel, "Study of the PbO₂/Pb²⁺ Cycling in Methanesulfonic Acid Medium for Soluble Lead(II) Flow Battery Application", lecture held by A. Oury during the 221st ECS Meeting - Seattle, Washington, May 6 - May 10, 2011

Poster communications

1. A. Kirchev, D. Pavlov and B. Monahov, "A method for investigation of the stationary electrochemical kinetics of O₂ recombination in valve regulated lead acid (VRLA) batteries", poster presented by A. Kirchev during the International Workshop "Advanced Techniques for Energy Sources Investigation and Testing", 4th - 9th September 2004, Sofia, Bulgaria
2. D. Valkovska, D. Pavlov, A. Kirchev, "Heat generation in VRLA battery – influence of separator type" poster presented by A. Kirchev during the 6th International conference LABAT'2005, 13-16 June 2005, Varna, Bulgaria
3. A. Kirchev, F. Mattera, J. Merten, "Impedance characterization of silicon PV cells and modules", poster presented by J. Merten during the 22nd European Photovoltaic Solar Energy Conference, 3-7 September 2007, Milan, Italy, p. 360
4. T.K. Dong, A. Kirchev, F. Mattera, A. Delaille, "Integration of lithium-ion battery in photovoltaic applications: Impedance characterization and electric equivalent circuit modelling", poster presented by A. Delaille during the Advanced Automotive Battery Conference, 14-16 May 2008, Tampa, Florida, USA
5. N. Martin, Z. Feng, M. Perrin and A. Kirchev, "Equivalent electric circuit based simulation of Ni-MH batteries for renewable energy storage", poster presented by M. Perrin during the 4th International Renewable Energy Storage Conference IRES 2009, November 24-25, 2009, Berlin, Germany
6. N. Martin, A. Kirchev, M. Perrin, J. Rolling, R. Manzoni and G. Crugnola, "Testing and modelling of ZEBRA batteries for grid-connected PV applications", poster presented during the 5th International Renewable Energy Storage Conference IRES 2010, November 22-24, 2010, Berlin, Germany

Acknowledgements

I would like to thank the whole team of Laboratoire de Stockage de l'Electricité for the past eight years of working together – time went really fast and the results in this manuscript are results of us all. I would like to thank also to the Lead-Acid Battery Department of the Institute of Electrochemistry and Energy Systems (former CLPS) and to Dr Boris Monahov, in particular, for getting me in the craft of the lead-acid batteries.

I would like to acknowledge sincerely the support of my ideas and visions about the electrochemical energy storage received from my superiors Dr Florence Lambert, Dr Jens Merten and Dr Marion Perrin. Great part of the results above was due to their decisions as managers.

Sincere thanks to the members of the jury for this HDR Dr Christine Lefrou, Professor François Huet, Dr Emmanuel Rocca, Professor Patrice Simon, and Dr Pat Moseley and last but not at least Professor Detchko Pavlov, my first teacher in energy storage and electrochemistry. Your willingness and commitment to evaluate the results of my work as reviewers and examiners are highly appreciated.

I would like to acknowledge the patience and the dedication of all PhD and graduate students I worked with in INES. We learned much from each other.

I would like to thank Professor Yann Bultel and Dr Pascal Mailley for the numerous advices and tips in the preparation of this HDR.

I would like to thank my daughter Nikol and my wife Nina for the continuous curiosity and admiration for my work, which are my greatest inspiration. Благодаря ви от цялото си сърце МИЛО мое семейство!